



OsloMet – storbyuniversitetet
Institutt for Bygg- og energiteknikk - Bygg
Postadresse: Postboks 4 St. Olavs plass, 0130 Oslo
Besøksadresse: Pilestredet 35, Oslo
Telefon: 67 23 50 00 www.oslomet.no

MASTER THESIS

TITLE Mechanical reinforcement of cement pastes with Cellulose Acetate microfibers produced by electrospinning.	DATE 25.05.2023
	NO. OF PAGES 77
AUTHORS Manaab Zegeye T. Tedros Habteab B.	Supervisors Rafael Borrajo Mahdi Kioumars Sarrah Darssi, Saja Al-Batat
SUMMARY <p>Electrospun fibers have attracted attention due to their unique qualities and potential uses, such as construction. This study aimed to assess how PVP/TEOS and CA microfibers could affect the mechanical properties of cement composites. Still, the PVP/TEOS fibers disintegrated in water during the experimental phase. This project examined the effect of cellulose acetate (CA) fibers on composite properties. Experimental results showed that CA significantly improved compressive strength at seven days, while lower compressive and flexural strength was observed after 28 days of curing. Future works are needed to explore solutions for better dispersion of CA fibers in cement-based materials to maximize the beneficial effects of CA-microfiber reinforcement.</p>	

KEYWORDS
Electrospinning
Fiber reinforced composites

Acknowledgment

This thesis is a conclusion of our master's in structural and civil engineering and prepared for the Faculty of Technology Art and Design (TKD) and the Faculty of Mechanical, electronics, and chemical engineering (MEC) at Oslo Metropolitan University (OsloMet). This work is carried out within six months, from January to May 2023, and counts for 30 credits. In addition, this thesis is a collaborative work and study between authors/students at OsloMet, Tedros Habteab, and Manaab Zegeye.

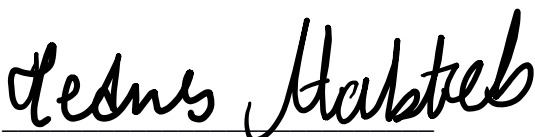
We want to express our appreciation to all those who have provided support, assistance, and valuable contributions to the completion of this thesis. Firstly, we sincerely thank our supervisors, Associate Professor Rafael Borrajo, Associate Professor Mahdi Kioumarsi, and Associate Professor Sarra Drissi from Oslo Metropolitan University (OsloMet). Their expertise, guidance, and strong support have been instrumental in shaping the direction and quality of this research. We immensely thank their continuous assistance and inspirational insights throughout this journey.

We sincerely thank our family for their unwavering support, love, and understanding during our academic career. Their consistent encouragement has been a steady source of inspiration. Additionally, we want to thank our friends and colleagues for their support and assistance. Their support, conversations, and idea-sharing have helped form our research.

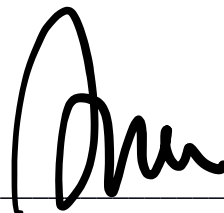
A special mention goes to Saja Al-Batat, the Concrete Lab engineer from the Civil Engineering Department, for her assistance and support during the experimental phase of our research. A special mention goes to Ingrid Gigstad, senior engineer at OsloMet Chemistry Lab, for holding an introductory instruction course to use laboratory and chemical management safely. Their expertise and willingness to share their knowledge have been invaluable in ensuring the smooth execution of our laboratory experiments. We sincerely thank Associate Professor Shima Pilehvar, Associate Professor Susana Garcia, and the Department of Engineering at Østfold University College for providing laboratory resources and support throughout the thesis.

Finally, we would also like to thank Rune Orderløy for his enormous technical support in setting up the inbox, training microscope, and logistics accommodation.

Once again, we would like to express our sincere gratitude to everyone who helped make this thesis a reality, including those we already mentioned. Your help and support have been excellent, and we sincerely appreciate it.



Tedros Habteab



Manaab Zegeye

Oslo, 25.05.2023

Abstract

Electrospun fibers have attracted much attention in various industries due to their distinctive qualities and possible uses, including construction. Electrospinning produces ultrafine fibers by exposing a polymer solution or melting to a high-voltage electric field. These fibers' nanoscale to micrometer sizes provides remarkable mechanical qualities and a high surface area-to-volume ratio. Electrospun fibers offer several benefits and modern advancements in the building construction industry, including increased strength and durability, improved energy efficiency, and environmental sustainability. The usage of electrospun fibers in the construction sector is still constrained, and areas still require improvement. Examples include pertinent parameters, scaling-up challenges, standardization, and regulations. As a result, the master has directed their efforts toward assessing a friendly method for the electrospinning process and innovative cement composites by reinforcing them with microfibers produced by their hand in the OsloMet Chemistry Lab to enhance flexural and compressive strength.

Initially, two different fibers, mainly cellulose acetate (CA) and polyvinylpyrrolidone/tetraethyl orthosilicate (PVP/TEOS), were considered for this study. These fibers were produced through a process called electrospinning, which involves the use of electrical forces to create delicate and continuous fibers. The objective was to assess how different types of fibers could affect the mechanical properties of composites made of cement. However, the PVP/TEOS fibers disintegrated in water during the experimental phase, making them unsuitable for further investigation. Therefore, only cellulose acetate (CA) fibers were considered for this project.

Three different mixes were prepared to examine the effect of CA on the final composite's properties, each containing varying amounts of CA fibers: 0.1%, 0.5%, and 1%. Experimental results showed that CA significantly improved compressive strength at an early age. For instance, adding 1% CA fibers increased the 7d compressive strength by 13,8%, whereas adding 0.1% and 0,5% CA fibers improved compressive strength by 9.4% and 2,9%, respectively. This could be attributed to the increased interfacial interaction between CA fibers with the cement paste matrix. In contrast, lower compressive strength was observed after 28 days of curing. Similar results were noticed for flexural strength after 7 and 28 days. This was mainly attributed to the agglomeration of CA fibers within the cement paste. These agglomerated CA fibers give rise to regions of weak spots in the form of pores. On the other hand, it could generate additional macropores and thus weaken the cement matrix. Future works are needed to explore solutions for better dispersion of CA fibers in cement-based materials to maximize the beneficial effects of CA-microfiber reinforcement.

In summary, this work highlights the potential use of electrospun fibrous additives in composites based on cement. The results open new avenues for investigation and development in this unexplored field, enabling the development of innovative, high-performance building materials that can satisfy the strict demands of modern construction.

Content

ACKNOWLEDGMENT	2
ABSTRACT	3
CONTENT	4
LIST OF FIGURES	6
LIST OF TABLES	8
1 INTRODUCTION	9
1.1 GENERAL BACKGROUND	9
1.2 RESEARCH OBJECTIVE.....	11
1.3 SCOPE	11
1.4 LIMITATION	12
2 METHOD	14
OVERVIEW	14
2.1 FIRST STEP - SELECTION OF DATABASE	14
2.2 SECOND STEP - KEY CONCEPTS AND PRIMARY SEARCH.....	14
2.3 THIRD STEP - CONTENT ANALYSIS	15
3 LITERATURE REVIEW	18
3.1 PROCESS AND MECHANISM	18
3.2 ELECTROSPINNING METHODS	19
3.3 ELECTRO-SPINNABLE MATERIALS AND AGENTS	22
3.4 ELECTROSPUN FIBERS PROPERTIES.....	23
3.5 RELEVANT PARAMETERS.....	24
3.6 INSTRUMENTS	26
4 EXPERIMENTAL PROGRAM CA AND PVP NANOFIBERS	29
4.1 NANOFIBER PRODUCTION.....	29
4.2 CHEMICALS AND REAGENTS	30
4.3 PVP/TEOS	30
4.4 CELLULOSE ACETATE (CA)	31
4.5 PREPARATION OF MATERIALS	32
5 OPTIMIZATION AND CHARACTERIZATION OF MICROFIBER PROPERTIES	33
5.1 MEASUREMENT ERROR.....	33
5.2 PVP/TEOS FIBER WITH POSITIVE VOLTAGE APPLICATION.....	34
5.2.1 <i>Flow rate effect</i>	34
5.2.2 <i>Distance effect</i>	36
5.2.3 <i>Voltage effect</i>	38
5.3 CA FIBERS WITH POSITIVE VOLTAGE APPLICATION.....	40
5.3.1 <i>Flow rate effect</i>	40
5.3.2 <i>Distance effect</i>	41
5.3.3 <i>Voltage effect</i>	42
5.4 PVP/TEOS FIBERS WITH NEGATIVE VOLTAGE APPLICATION	43
5.4.1 <i>Flow rate effect</i>	43
5.4.2 <i>Distance effect</i>	44
5.4.3 <i>Voltage effect</i>	45

5.5	CA FIBERS WITH NEGATIVE VOLTAGE APPLICATION.....	46
5.5.1	<i>Flow rate effect</i>	46
5.5.2	<i>Distance effect</i>	46
5.5.3	<i>Voltage effect</i>	47
6	MICROFIBER OPTIMIZATION RESULT.....	49
6.1.1	<i>Flow Rate Effect</i>	49
6.1.2	<i>Emitters Distance Effect</i>	51
6.1.3	<i>Voltage effect</i>	53
7	CEMENTITIOUS COMPOSITE.....	56
7.1	MATERIALS AND SAMPLE PREPARATION.....	56
7.2	SAMPLE PREPARATION.....	56
7.3	TEST METHODS.....	57
7.3.1	<i>Compression strength test</i>	57
7.3.2	<i>Flexural strength test</i>	58
8	RESULTS AND DISCUSSIONS.....	60
8.1	CELLULOSE ACETATE (CA) MICROFIBER.....	60
8.2	EFFECT OF CA-MICROFIBER COMPOSITE ON THE PROPERTIES OF THE PASTE.....	62
8.2.1	<i>Compressive strength</i>	62
8.2.2	<i>Flexural strength</i>	64
9	CONCLUSION.....	70
10	RECOMMENDATIONS FOR FUTURE WORK.....	72
11	REFERENCE.....	73

List of Figures

FIGURE 3-1. FORCES-ACTING-ON-A-TAYLOR-CONE-DURING-ITS-ELECTRO-JETTING-PROCESS.PNG	18
FIGURE 3-2. EXAMPLES OF DIFFERENT CONFIGURATIONS IN NEEDLE-BASED AND NEEDLE-LESS ELECTROSPINNING.	20
FIGURE 3-3. EXAMPLE OF HORIZONTAL, NEEDLE-BASED ELECTROSPINNING WITH A SINGLE-NEEDLE.....	21
FIGURE 3-4. ELECTROSPINNING INSTRUMENT ‘ ‘ SPINBOX AND SYRINGE PUMP’ USED FOR THE EXPERIMENT.	27
FIGURE 4-1 CHEMICALS AND REAGENTS USED IN THESIS.	30
FIGURE 4-2. RAW ELECTROSPUN MICROFIBERS	31
FIGURE 4-3. MICROSCOPIC VISUALIZATION OF THE PVP/TEOS MICROFIBERS IN WATER	31
FIGURE 4-4. POLYMER JET BEFORE THE COAGULATION STARTS.	32
FIGURE 4-5. THE EARLY STAGE OF COAGULATION.....	32
FIGURE 5-1. OPTICAL MICROSCOPE OLYMPUS GX71	33
FIGURE 5-2. MESURMENT FOR THE OUTER DIAMETER	34
FIGURE 5-3. ACTUAL STANDARD SIZE FOR GAUGES IN THE MARKET.	34
FIGURE 5-4. MEASUREMENT FOR THE OUTER DIAMETER.....	34
FIGURE 5-5. ILLUSTRATION OF GAUGE 22	34
FIGURE 5-6. MICROFIBERS MADE OF PVP/ETHANOL/TEOS [6G - 30G - 4.60G] DIAMETER ILLUSTRATION CHART.	35
FIGURE 5-7. MICROFIBERS MADE OF PVP/ETHANOL/TEOS [1.55G - 15G - 2.34 G] DIAMETER ILLUSTRATION CHART.....	36
FIGURE 5-8. MICROFIBERS MADE OF PVP/ETHANOL/TEOS 3 G: 15 G: 2.34 G DIAMETER ILLUSTRATION CHART.....	37
FIGURE 5-9. MICROFIBERS MADE OF PVP/ETHANOL/TEOS [1G: 5G: 0.78G] DIAMETER ILLUSTRATION CHART.	38
FIGURE 5-10. MICROFIBERS MADE OF PVP/ETHANOL/TEOS G18 [1G: 5G: 0.78G] DIAMETER ILLUSTRATION CHART.....	39
FIGURE 5-11. MICROFIBERS MADE OF CA/ ACETATE [12.5 G -100ML] DIAMETER ILLUSTRATION CHART.	40
FIGURE 5-12. MICROFIBERS MADE OF CA/ ACETATE [12.5G - 87.5G] DIAMETER ILLUSTRATION CHART.	41
FIGURE 5-13. MICROFIBERS MADE OF CA/ACETATE [12.5 G, 87.5 ML] DIAMETER ILLUSTRATION CHART.	42
FIGURE 5-14. MICROFIBERS MADE OF PVP/ETHANOL/TEOS [3 G -15 G -2.34 G] DIAMETER ILLUSTRATION CHART.....	43
FIGURE 5-15. PVP/ETHANOL/TEOS [3 G: 15 G: 2.34 G]	44
FIGURE 5-16. PVP/ETHANOL/TEOS [1G: 5G: 0.78G].....	45
FIGURE 5-17. MICROFIBERS OF CA/ACETATE [12.5 G: 100 ML] DIAMETER ILLUSTRATION CHART.	46
FIGURE 5-18. MICROFIBERS MADE OF CA/ACETATE [12.5 G: 100 ML] DIAMETER ILLUSTRATION CHART.	47
FIGURE 5-19. MICROFIBERS MADE OF CA/ACETATE [12.5 G: 100 ML] DIAMETER ILLUSTRATION CHART.	48
FIGURE 6-1. RESULT FROM CA -C-G15-F	50
FIGURE 6-2. RESULT FROM PVP/TEOS -B-G18-F.....	50
FIGURE 6-3. RESULT FROM PVP/TEOS -A-G18-F.....	50
FIGURE 6-4. RESULT FOR THE FLOW RATE EFFECT CA-C-G15-F	51
FIGURE 6-5. THE RESULT FOR THE FLOW RATE EFFECT PVP-A-G15-F.....	51
FIGURE 6-6. RESULT FOR DISTANCE EFFECT CA-D-G15-D	52
FIGURE 6-7. RESULT FOR DISTANCE EFFECT PVP-A-G15-D	52
FIGURE 6-8. RESULT FOR DISTANCE CA-C-G15-D.....	52
FIGURE 6-9. RESULT FOR DISTANCE PVP-A-G15-D.....	52
FIGURE 6-10 RESULT FOR THE VOLTAGE EFFECT CA-C-G15-V	53

<i>FIGURE 6-11. RESULT FOR THE VOLTAGE EFFECT PVP-A-G18-V</i>	53
<i>FIGURE 6-12. RESULT FOR THE VOLTAGE EFFECT PVP-B-G18-V</i>	54
<i>FIGURE 7-1. MOLDS AND SAMPLES USED IN THIS EXPERIMENT</i>	56
<i>FIGURE 7-2. ADMIXTURE CEMENT/MICROFIBER DEMONSTRATION</i>	57
<i>FIGURE 7-3. COMPRESSION TESTING MACHINE</i>	58
<i>FIGURE 7-4. ILLUSTRATION FOR THE FLEXURAL STRENGTHS TESTING PROCESS</i>	59
<i>FIGURE 8-1 COMPRESSIVE STRENGTH RESULT FOR 7D AND 28D</i>	63
<i>FIGURE 8-2 RESULT FOR THE FLEXURAL STRENGTH RESULT FOR 7D AND 28D</i>	65
<i>FIGURE 8-3 OBSERVED AGGLOMERATED CA-FIBER AND WEAK SPOTS IN THE CEMENT SAMPLES AFTER BEING TESTED</i>	66
<i>FIGURE 8-4 SEM IMAGES OF THE SAMPLES CONTAINING 0.5% CA (C & D) AND 1% CA (A & B). IMAGES (A) & (C) VISIBLE AGGLOMERATION OF FIBERS. IMAGES (B) & (D) SHOW NO OBSERVABLE FIBERS.</i>	67
<i>FIGURE 8-5 AVERAGE PEAK LOAD AT 7D AND 28D</i>	68
<i>FIGURE 8-6 LOAD VERSUS DEFORMATION AT 28D</i>	69

List of Tables

<i>TABLE 1-1. OUTLINE OF THIS MASTER THESIS.</i>	12
<i>TABLE 2-1. KEY CONCEPT FOR ELECTROSPINNING PROCESS.</i>	15
<i>TABLE 2-2. KEY CONCEPT FIBER REINFORCED CEMENT COMPOSITE.</i>	15
<i>TABLE 2-3. CATEGORIZATION OF THE LITERATURE REVIEW.</i>	16
<i>TABLE 3-1. EXPERIMENTAL PLAN FOR PARAMETERS</i>	28
<i>TABLE 4-1. DESCRIPTION OF THE POLYMER CONCENTRATION USED IN THIS EXPERIMENT.</i>	29
<i>TABLE 4-2. DESCRIPTION OF CODE ADOPTED IN THE EXPERIMENT WITH POSITIVE HIGH VOLTAGE.</i>	29
<i>TABLE 4-3. DESCRIPTION OF CODE ADOPTED IN THE EXPERIMENT WITH NEGATIVE HIGH VOLTAGE.</i>	29
<i>TABLE 6-1. FLOW RATE EFFECT WITH THE POSITIVE VOLTAGE FOR THE PVP/TEOS AND CA MICROFIBERS</i>	49
<i>TABLE 6-2. FLOW RATE EFFECT WITH NEGATIVE VOLTAGE FOR PVP/TEOS AND CA MICROFIBER</i>	50
<i>TABLE 6-3. THE TIP-TO-COLLECTOR DISTANCE EFFECT WITH POSITIVE VOLTAGE.</i>	51
<i>TABLE 6-4. THE TIP-TO-COLLECTOR DISTANCE EFFECT WITH NEGATIVE VOLTAGE.</i>	52
<i>TABLE 6-5. THE POSITIVE-VOLTAGE EFFECT IN PVP/TEOS AND CA MICROFIBER.</i>	53
<i>TABLE 6-6. THE TIP-TO-COLLECTOR DISTANCE EFFECT WITH NEGATIVE VOLTAGE.</i>	54
<i>TABLE 6-7. MOST PROMISING PARAMETERS FOR THE RESEARCH</i>	55
<i>TABLE 8-1 COMPRESSIVE STRENGTH TEST RESULTS AT 7D AND 28D.</i>	63
<i>TABLE 8-2 FLEXURAL STRENGTH TEST RESULTS AT THE AGE OF 7D AND 28D.</i>	65

1 Introduction

1.1 General background

Cementitious materials, mainly concrete, have been essential for the construction industry's infrastructure development for centuries. Although tensile strength, crack resistance, and durability of typical concrete are constrained. Therefore, the electrospinning method and its use in cementitious materials have recently attracted much interest due to its potential to improve construction materials' mechanical qualities and durability. Several key benefits can be achieved by introducing electrospun fibers into cementitious materials. Our thesis will consider some of them, “flexural and compressive strength for the fiber-reinforced cement composite,” which are essential in structural building engineering. At the same time, the electrospinning process will be investigated and experimented deeply.

Electrospinning process

The phrase "electrospinning" is derived from "electrostatic spinning." It is a high-voltage-driven fabrication technique that produces tiny fibers from a polymer solution and is governed by chamfered and conventional flat-end nozzle electrohydrodynamic phenomena. When Darrell Reneker and Gregory Rutledge reintroduced this technique nearly 30 years ago (around 1994), the increasing availability of electron microscopes capable of resolving details down to the nanometer scale allowed for greater flexibility in surface functionalities and superior mechanical performance (such as stiffness and tensile strength) compared to any other known material form [1]. Chemistry and polymer science advanced concurrently with the introduction of synthetic fiber around 1961.

DuPont made nylon commercially available in 1938, piquing the public's interest. Following that, numerous varieties of polyesters and other synthetic polymers were developed to produce synthetic fibers. Synthetic fibers vastly expand the range of applications while decreasing the public's demand for natural fibers [2]. Several techniques, such as needle-based electrospinning, are commonly used to create fibers from synthetic polymers. The most basic setup for this technique consists of a solution in a reservoir — typically a syringe — tipped with a blunt needle (at least for needle-based electrospinning), a pump, a high-voltage power source, and a collector [2].

The process involves extruding polymer solution into the air via a spinneret (in the form of jets), and "electrospun fibers" are generated via solvent evaporation with the assistance of a hot air stream[3-6]. The potential difference of electrospun fibers is determined by the spinning fluid's properties, such as viscosity and polymer molecular weight.

Furthermore, changing the concentration changes the shape of the electrodeposited coating from a beaded coating to a filamentous coating, as well as the morphology [7]. Other factors that may influence fiber production include technical properties such as strength, voltage, and polarity of the electric field, as well as the distance between the needle and collector[8-10].

Between 1964 and 1969, Geoffrey Taylor published a series of groundbreaking papers describing how to mathematically represent and simulate the transformation of a polymer solution or melt droplet's shape from spherical to conical under the influence of a strong electric field[11]. As the strength of the electric field was increased above a certain level, the spherical droplet would gradually change into a cone (now known as the Taylor cone) [12] and emit a liquid jet [2, 4, 13, 14]

After being discharged from a metal spinneret with a tiny hole, the charged solution jets evaporated, forming fibers and accumulating on the collector[15-21]. Electrospun fibers can be made from various materials, depending on the application. Polymers, such as industrial polymers, biodegradable polymers, specialty polymers, and natural polymers, are the most used materials for electrospinning. Simultaneously, carbon nanofiber composite materials for applications such as space engineering and automotive industries are critical due to their high mechanical properties.

On the other hand, Electro-spinnable polymers can be used to routinely create polymer matrix nanofiber composites, primarily through a blending technique that includes fillers with the solution before electrospinning[22-26].

Researchers experimented with adding polymers such as Nylon 66, TEOS/PVP, CNTs-TEOS/PVP, cellulose acetate (CA), and other materials to the cement paste, which resulted in covering the surface of the hydration product and filling cracks and holes, increasing the mechanical strength of the hardened cement matrix[27-30]. Concrete is the world's most used building material and one of the essential materials we have because of its affordability, use of widely available raw materials, and excellent mechanical strength; however, the frequent occurrence of cracks in the cementitious matrix, which lowers the overall strength of the material, is a disadvantage of this composite material. As a result, fibers were incorporated into the mix design to improve the tensile and flexural properties of the material and prevent cracking [29]

However, very few studies have used polymers or fibers driven by the electrospinning process in the cementitious matrix. As a result, the current thesis aims to identify the potential of cellulose Acetate CA and Polyvinylpyrrolidone Tetraethoxysilane PVP/TEOS polymers based electrospun to enhance

the mechanical properties of cementitious constructions. Furthermore, it comprehends the electrospinning process and other factors influencing the manufacturing of cement composite.

1.2 Research objective

There are two critical objectives for our research. First, we want to learn more about electrospinning and investigate the best settings for producing microfibers with a minor feasible diameter. Second, we want to examine how adding these microfibers to a cement composite affects its mechanical characteristics.

1. Study the electrospinning procedure: Examine the electrospinning procedure in detail, paying particular attention to the variables that affect fiber diameter. To produce microfibers with a possible minor diameter, it is necessary to assess several variables, including solution viscosity, applied voltage, needle size, and spinning distance.
2. Optimize the fiber spinning parameters by identifying the critical factors that significantly impact fiber diameter during electrospinning through experimental testing and analysis. To fabricate micro/nanofibers is essential to thoroughly grasp how changes in these parameters affect the resultant fiber morphology and diameter.
3. Evaluate the effect on the mechanical properties: Analyze the impact of adding electrospun microfibers on the mechanical characteristics of a cement composite. Conduct thorough testing to evaluate the composite material's compressive strength, flexural strength, and impact resistance under (0.1%, 0.5%, and 1%) microfiber reinforcement levels. To evaluate the improvement in mechanical performance, compare these parameters to those of the unreinforced cement composite.
4. Determine potential uses and advantages: Based on its increased mechanical properties, evaluate the advantages and future uses of the microfiber-reinforced cement composite. Examine the benefits of the composite material's improved compressive and flexural strength.

By achieving these study goals, we aim to advance knowledge of the electrospinning method used to create microfibers and how it affects the mechanical characteristics of cement composites. The research's conclusions will offer helpful information for enhancing the manufacture of microfibers and making high-performance composite materials for various applications.

1.3 Scope

This master's thesis aims to enlighten the advantages and capacity of polymeric micro/nanofibers to improve the mechanical properties of cementitious materials. At the same time, introduce electrospun

fibers as a sustainable alternative to natural fibers and steel fibers to develop fiber-reinforced cement composite. Furthermore, it will assess the physical properties of the electrospun fibers during the electrospinning process and its feasibility in improving the flexural and compressive strength of the cementitious material. *Table 1-1* below presents the outline of this master thesis.

Table 1-1. Outline of this master thesis.

Outline of this master thesis	
Chapter 1 Introduction	Briefly description of microfiber and cement paste General background, the research objective, the scope and limitations of this thesis
Chapter 2 Method	A description of how the literature review methods of choosing databases and relevant articles were utilized.
Chapter 3 Literature review	This chapter contains a detailed review of articles to support the experimental work in this thesis.
Chapter 4 Experimental program CA and PVP nanofibers	The CA and PVP microfiber experimental program, preparation and production phase are described here.
Chapter 5 Optimization and characterization of microfiber properties	Optimization and characterization of the microfibers are presented in detail in this chapter. A detailed explanation of the experimental investigation and presentation of the results.
Chapter 6 Microfiber optimization result	The result of the optimized microfiber used in further work is presented here.
Chapter 7 Experimental program cementitious composite	The experimental program of cement paste reinforced with CA microfiber, preparation, and casting method are described in this chapter.
Chapter 8 Result and discussion	Presentation of all the various findings and explanation of them in connection to the fundamental theory.
Chapter 9 Conclusion	The significant results from the experiments are detailed in this chapter, and the researcher's questions and related questions are thoroughly addressed.
Chapter 10 Recommendations for future work	Recommendations for future studies in the relevant field are included in this chapter.
Reference	A comprehensive reference list includes a list of all the sources utilized in the thesis.
Appendix	In this chapter, the appendices of the thesis are included, such as digital microscope photos of the fibers.

1.4 Limitation

Despite our best efforts, several restrictions had a significant impact on our work. Although it was not our intention to blame, these restrictions clearly had an effect on the results we were able to produce. Here are some of the main obstacles we encountered:

1. Restricted access to the Spinbox room: We needed help entering the room, which required us to wait unnecessarily for someone to open it. This time may have been used to increase the

output of the fibers. Our progress could have been better, and perhaps our work quality suffered from the absence of timely access.

2. Delayed access to the microscope and lab room: Like the Spinbox room, the microscope and lab room also experienced delays in access. These delays made it difficult to complete crucial tests and analyses on time.
3. Limited software access: During a significant amount of production time, only one student had access to the necessary software. This limited access made collaborating difficult and slowed the project's overall pace. As a team, members could not participate as much as they would have, which might have influenced the final results and efficiency of our work.
4. Inadequate visualization abilities: The requisite visualizations could be achieved with a scanning electron microscope (SEM). With this essential tool, we were able to create precise and thorough graphic representations of our samples. The depth and comprehensiveness of our conclusions may have been constrained by this limitation, making it difficult to assess and interpret several parts of our research.

Even though these restrictions have had an influence on our work, it is essential to note that we have made every effort to address these issues within the limitations that have been imposed. By being aware of these limits, we may better comprehend the variables that affected our results and pinpoint areas where future projects can be improved.

2 Method

Overview

This master's thesis experimental investigation is mainly based on a literature review completed during the specialization course "MABY5010- Specialization in Structural Engineering and Building Technology" last semester. The systematic content review on the assessment of "*Mechanical reinforcement of building materials with microfiber produced by electrospinning*" was conducted using a three-step study technique. Choosing a database, creating key concepts and search terms, and doing a literature review are all steps in this technique. A set of search strings and sentences was created based on the developed key concepts [Table 2-1](#) and [Table 2-2](#).

2.1 First step - Selection of database

The first step involved choosing relevant and accurate articles on the research topic - "Mechanical reinforcement of building materials with nanofibers produced by electrospinning" - from three reliable databases:

1. Scopus (scopus.com)
2. Web of Science (webofscience.com)
3. ScienceDirect (sciencedirect.com)

Credibility was one of the factors that led to the selection of these databases. The combination of the results from all of them produces a high coverage of articles pertinent to the subject of this study and reduces the likelihood that an article will be missed. The work was extensive since the study field is still relatively new. The experiment is split into two parts: 1. manufacturing electrospun nanofiber and 2. mechanical reinforcement cement paste using electrospun nanofibers. Therefore, it was necessary to find articles outside the above databases because it took time to find relevant enough articles focusing on mechanical reinforcement cement paste using electrospun nanofibers.

2.2 Second step - Key Concepts and Primary Search

Several keywords were generated to perform a planned and systematic search. These keywords were used as the first criterion to check the search results. Some of the keywords included are presented in [Table 2-1](#) and [Table 2-2](#).

Table 2-1. Key concept for electrospinning process.

Key concepts		
Concept 1	Concept 2	Concept 3
Nanofiber	Possessing parameter	Electrospinning
Cellulose acetate polymer	High voltage	Electro fiber spinning
Polypropylene	Flow rate	Electro-fiberization
Polystyrene	Tip-to-collector distance	Electro-fiber spinning
Nylon	Spinnability	Electrostatic spinning
TEOS/PVP	Solubility	Taylor cone
Carbon nanotubes (CNTs)	Mathematical parameters	
Polyacrylonitrile (PAN)		

Table 2-2. Key concept fiber reinforced cement composite.

Key concepts		
Concept 1	Concept 2	Concept 3
Mechanical enhancement	lime mortar	Fiber reinforced cement
Mechanical properties	Ordinary cement	Polymer fiber
Tensile strength	Hydrated lime	
Toughness	Disintegration	
durability	Cement paste	
Flexural strength		
Compressive strength		

Different categories for the various literature searches were created. Boolean operators like "OR" and "AND" were then utilized to merge the keywords into a search string/ phrase for each literature search by integrating these concepts. In order to focus on articles that had been published in those databases, our search was limited to " English-language publications" while reducing the number of duplicates. For example, several articles were visible on Scopus, but these were also published in other databases, which would have led to a duplicate list of articles.

2.3 Third step - Content Analysis

A third step was required to effectively manage the articles obtained from the first two processes and remove duplicates and less critical articles that had yet to be filtered out in the first two steps. A review and manual filtering of the articles was carried out, which reduced the number of articles after removing duplicates. As noted, this study paper is divided into two sections: creating the fibers and using those fibers to reinforce cement paste. Therefore, the articles were categorized in *Table 2-3* according to the study area and functioning to handle them better and more straightforwardly.

Table 2-3. Categorization of the literature review.

Category	Amount	Percent	Source
Process and mechanism	10	12,3	[3, 4, 11, 14, 15, 17, 20, 31-33]
Electrospun nanofiber and Area of application	9	11,1	[1, 2, 5, 7, 24, 34-37]
Parameters effect in electrospinning	11	13,6	[8, 13, 18, 38-45]
Spinnable material and agents	13	16,0	[9, 10, 16, 19, 21-23, 25, 26, 46-49]
Electrospinning Instrument	2	2,5	[6, 12]
Characterization and morphology	13	16,0	[50-62]
Technology and feature	4	4,9	[63-66]
Fiber-cement composite	14	17,3	[27-30, 67-72]
Pictures	5	6,2	[73-76]

Process and mechanism: Articles focusing on spinning techniques and the general idea of electrospinning.

Electrospun nanofiber and Area of application: These papers concentrate on the structure, characterization, and applications of electrospun polymer nanofibers. The articles may discuss production-related operations but mostly focus on electrospun polymer nanofibers and their potential applications.

Parameters effect in electrospinning: These articles focus on how various fibers' morphological and mechanical characteristics are affected by electrospinning parameters. The primary electrospinning parameters studied were needle-to-collector distance, voltage, polymer concentration, and solution flow rate.

Spinnable Material and Agents: The articles focus on the materials and agents used to produce fibers while describing the features and applications of nanofibers. However, the main focus is on materials and agents.

Electrospinning Instrument: The articles explore the evolution of nanofibers and the degree to which they have advanced to satisfy the demands of today's world. Both needle-based and needleless electrospinning technologies, which are currently used to create nanofibers, are described in the

publications. The articles provide an overview of the fundamental workings of several needle-based and needleless spinning technologies.

Characterization and morphology: Articles where the shape or structure of small diameters was examined, and the focus was on structure and morphology. The electrically driven jet, its instability, and its impact on the fiber shape may have been mentioned in the papers.

Technology and features: The articles discuss the fundamental ideas of polymers' physical, chemical, and mechanical techniques that can make them applicable to improving global lifestyles. They can also mention the potential for converting polymers into various composites and find wide-ranging uses in fields including biomedical engineering, solar cell manufacturing, energy generation, and environmental technology.

Fiber-cement composite: These papers investigate the application of nanofibers to modify cementitious materials' mechanical characteristics. Important topics like bending strength and compressive strength, which are the mechanical properties of the composite, are covered.

Standard: The standards for instructions and methods for casting and curing test specimens for strength testing. These are not articles but standards that must be followed.

3 Literature review

3.1 Process and Mechanism

Electrospinning begins when a specific voltage creates an electric field between the needle tip and the collector[2]. Charges accumulate on the liquid's surface while the pump keeps the solution flowing constantly. Soon, the electrostatic repulsion exceeds the surface tension, causing the liquid meniscus to deform into a Taylor cone [2]. Once the Taylor cone has formed, the charged liquid jet ejects towards the collector as the solvent gradually evaporates. The electrospinning process is divided into four significant steps that occur linearly.[2]

1. Liquid feeding system where the “Taylor cone-shaped jets create.”
2. Extension of the charged jet along a straight line
3. Thinning the jet in the presence of an electric field and growth of electrical bending instability (also known as whipping instability)
4. Solidification and, finally, collectors of the jet as solid fibbers in a grounded collector

A liquid feeding system and formation of Taylor cone

It is critical to understand the electrohydrodynamic mechanisms that govern the formation of a Taylor cone from an electrically charged liquid droplet. A syringe pump pumps the liquid into the spinneret at a predictable and steady rate during electrospinning. As the voltage rises gradually, more charges accumulate, increasing the density of surface charges on the droplet *Figure 3-1*. While electrostatic repulsion deforms the shape, increasing the surface area reduces repulsion. Surface tension, on the other hand, favors a spherical shape to reduce the sum of electrostatic and surface-free energy[21].

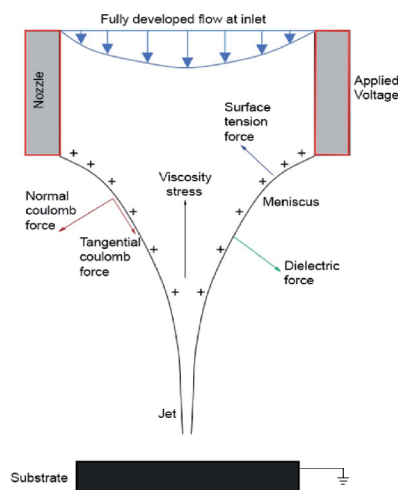


Figure 3-1. Forces-acting-on-a-Taylor-cone-during-its-electro-jetting-process.png

[77]

As a result, the droplet transforms from a hemisphere to a Taylor cone, with a powerful electric force concentrated at the tip of the Taylor cone. When the electric field reaches a particular value, the droplet at the cone tip overcomes surface tension. It expels into the electric field between the emitter tip and collector, forming a solution jet.

Extension of the charged jet along a straight line

It is unusual to come across polymer solutions that allow free electrons to move as they would in a metallic conductor. Polyaniline is an unusual exception[50], as electrons pass through dry polyaniline nanofibers. The tendency of the network of nanofibers to spread in the direction of the applied electric field rather than to produce a flat non-woven mat, as is typical of insulating polymers, highlighted the electrical conductivity of the polyaniline fibers during dry nanofiber collection. The electrons' characteristically quick redistribution time over the electrically conductive polyaniline nanofiber length caused this elongation. Electronic charge quickly collects and stretches the dry fiber network in the direction of the jet as it descends at close to 1 m/s at favorable fiber ends or bends[31].

Thinning of the jets, also known as whipping instability

During straight-line acceleration, the jet's surface tension and viscoelastic force prevent it from moving forward[21]. As a result, the acceleration gradually decreases. The diameter of the straight segment slowly shrinks as it moves away from the tip due to the jet's constant stretching. When the acceleration is zero or constant, any slight disturbance can stop a straight movement[38]. Because the electrostatic repulsion between the jet's surface charges has now entered the far-field region, instability can develop quickly.

Solidification, collector of the jets the as solid fibber's "electrospun"

The jet solidifies during the elongation process and transforms into fiber, caused by solvent evaporation or melt cooling. When the solidification process is slow, the charged jet can elongate for a more extended period, producing fibers with a narrower diameter. According to one study, stretching and solvent evaporation reduced the cross-sectional radius of a dry fiber to just 1.3×10^{-3} times that of the starting jet. After solidification, charges can still be held on the surface of dry fibers, but all instability is gone.

3.2 Electrospinning methods

Fibers can be produced by electrospinning through needle-based and needle-less electrospinning. For acknowledgment, a diagram is presented below in *Figure* to show the various available step options for both techniques and their versatility[21]. However, setups may make one more suitable for a

specific application than the other, while both are simple methods for producing functional nanomaterials. Despite this, the production of microfiber in this project will adopt the needle-based horizontal electrospinning method.

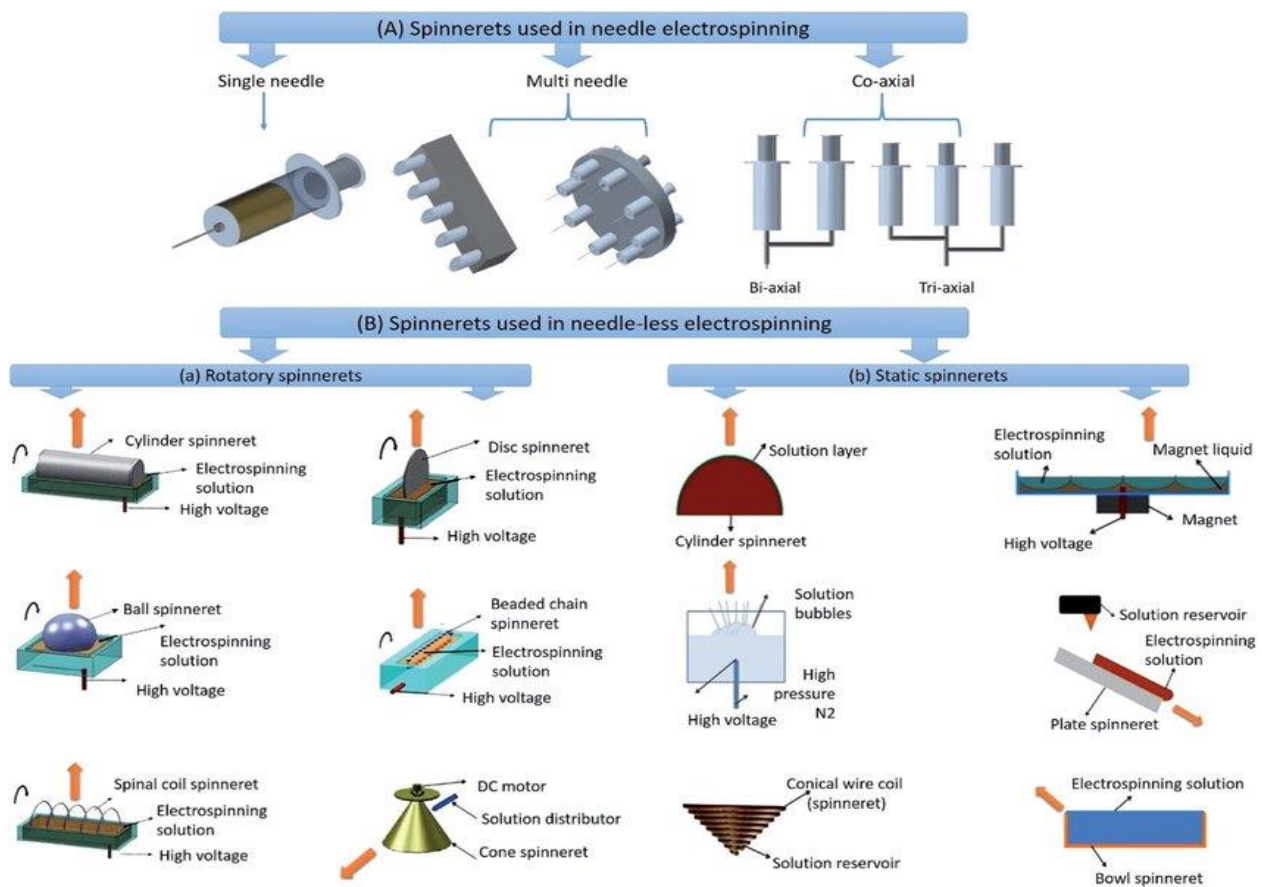


Figure 3-2. Examples of different configurations in needle-based and needle-less electrospinning.

[74]

Needle-based electrospinning

The development of a steady Taylor cone is an essential indicator of a stable and continuous electrospinning process. Therefore, capillary tube electrospinning (a needle, nozzle, or emitter) is required. Disposable polypropylene pipette tips and reusable Teflon or stainless-steel needles with a polypropylene hub connection are helpful for a successful electrospinning procedure.

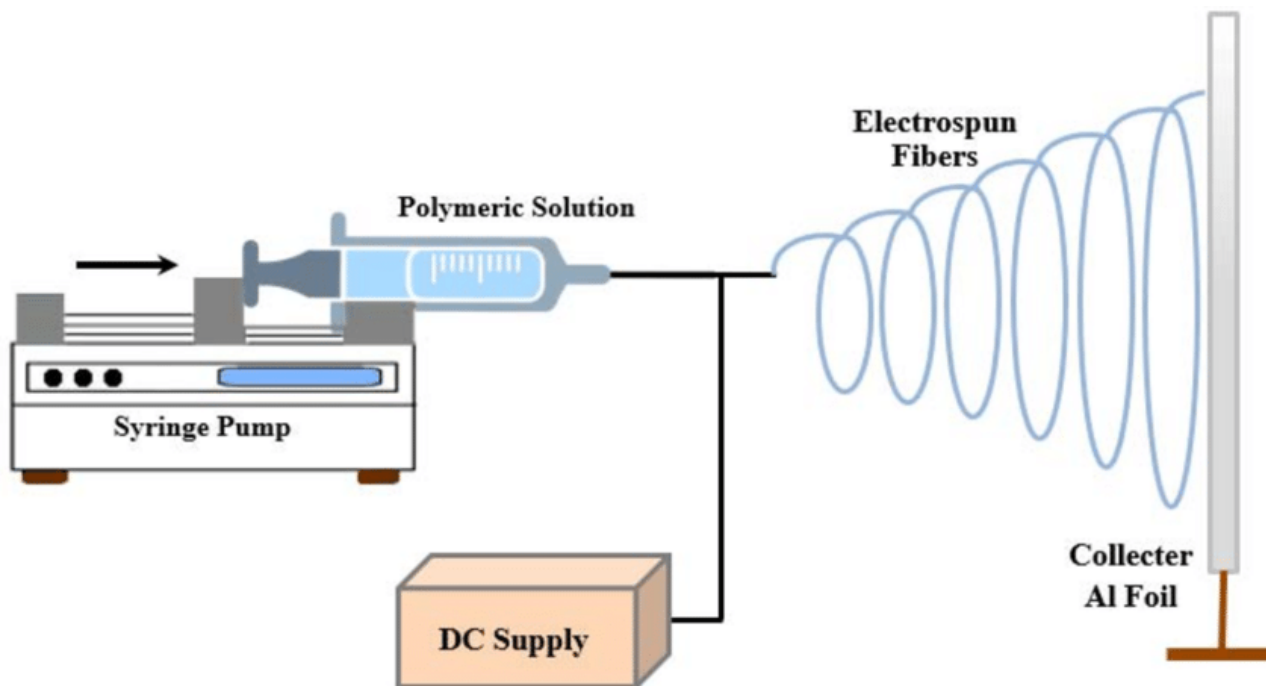


Figure 3-3. Example of horizontal, needle-based electrospinning with a single-needle

[76]

The solution is contained in an airtight and enclosed reservoir in needle-based electrospinning setups. This method ensures that the carefully crafted solution retains the desired properties such as concentration, viscosity, and surface tension. Once the processing parameters for sample development have been optimized, the enclosed solution's stability supports batch-to-batch consistency. For maximum batch-to-batch consistency and sample reproducibility, use new, well-mixed solutions that are no more than three days old. One of the primary benefits of keeping the solution contained is the safe use of various highly volatile substances such as chloroform, dichloromethane, and methyl acetate [21].

Each Taylor cone forms under ideal conditions where the solution flows constantly and the needle has a full charge (typically DC (Direct Current) high voltage). For industrial applications requiring high-throughput fabrication of nanomaterials, such as the Fluidnatek High-Throughput (HT) project, many configurations of multi-needle setups can be implemented with a few needles, dozens, or even thousands of needles. The number of needles introduced and the number of Taylor cones produced are directly related [34].

Horizontal Electrospinning

As shown in Figure 3-3, horizontal electrospinning is the most common orientation for processing electrospun. This processing method prevents gravity-driven drops from falling onto the collector and potentially contaminating the sample produced if a low-viscosity solution drips from the needle. [21].

3.3 Electro-spinnable materials and agents

Depending on the application, different polymers can be used to create electrospun fibers and various material properties must be considered. The electrospinning process can be altered to produce electrospun fibers with the desired morphology and characteristics. When mixed with other materials, the nanofibers can make a composite themselves. It can act as reinforcement in a matrix. To create ceramic fibers, post-processing procedures must follow electrospinning. Before selecting the appropriate electrospun fibers for applications, it is essential to have a fundamental understanding of the many types of materials [22].

Polymers

Polymer is the material that is electrospun the most commonly. Among the many kinds of polymers that have been electrospun are natural polymers, biodegradable polymers, specialty polymers, and industrial polymers. These polymers should generally have a high molecular weight and be solvent-soluble. Commercially significant polymers like polyethylene and polypropylene, which dissolve in few solvents, have an alternative in melt electrospinning. In order to spin other low-molecular-weight polymers, including polyaniline, it is frequently necessary to use a second sacrificial polymer that is also electrospinning-biopolymers, crosslinked polymers, conductive and nonconductive polymers, natural and synthetic polymers, etc. Most of the matrix materials used in composites are polymers. Several polymer matrices can be utilized to make composite materials. Among polymer matrix composites, thermoset matrix composites are more prevalent than thermoplastic composites. Thermoplastics and Thermosets have distinct properties and purposes despite the same name. Understanding performance disparities can help with improved sourcing decisions and composite product designs [63].

Carbon fibers

Because most polymers contain a carbon backbone, a post-electrospinning carbonization process can result in carbon nanofibers. Polyacrylonitrile is one of the most widely used polymers for converting to carbon (PAN). N, N-dimethyl formamide (DMF) works well as a solvent for electrospinning PAN

into nanofibers. Other polymers have also created carbon nanofibers via electrospinning and carbonization [23].

Metal oxide fibers

Many metal oxides have essential industrial uses because of their photoactivity and catalytic properties. Titanium dioxide, used in cosmetics, self-cleaning surfaces, and solar cells, is one of the most widely used metal oxides. Precursors can be electrospun alone or in combination with an electrospinnable polymer, such as polyvinyl pyrrolidone, to produce metal oxide nanofibers most frequently (PVP). The precursor used to make titanium dioxide is typically titanium isopropoxide. After that, a post-spin sintering process converts the precursor nanofibers into metal oxide nanofibers[24].

Metal fibers

Bulk metals are widely used as mechanical supports due to their incredible strength, but at much smaller dimensions, metals are more typically used as electrical conductors. The ability to create metal nanofibers enables the usage of nanowires in microelectronics. Metal nanowires cannot currently be produced by electrospinning directly, but it can be a stage in the process to do so. Additionally, electrospun fibers can be used as a template for metallic coating and subsequent sintering to produce metal tubes. Sputtering is a technique that can be used to coat electrospun nanofibers with a metallic coating to have a sufficiently thick and self-standing layer. Fibers made of polyethylene oxide were coated in palladium. Whole tubes must be created after sintering, necessitating at least 250 s sputtering periods. However, the thickness of the cylinder's wall portion is not uniform due to line-of-sight deposition[25].

3.4 Electrospun fibers properties

Molecular Orientation and alignment

Whether the electrospinning jet breaks into tiny droplets or produces electrospun fibers with beads depends significantly on the polymer chain entanglements[52]. Even though electrospinning demands a minimum amount of polymer chain entanglements, thus, a solution with too high viscosity will make it extremely difficult to pump the solution through the syringe needle [35]. Additionally, if the viscosity is too high, electrospinning may not start because the solution may dry at the needle tip. Numerous research shows that each polymer solution must have a minimum viscosity to produce fibers free of beads [53]. Beads are regularly observed at low viscosities along the fibers deposited

on the collection plate. Research shows that each polymer solution must have a minimum viscosity to produce fibers free of beads[53]. Beads are regularly observed at low viscosities along the fibers deposited on the collection plate.

Molecular weight

One factor affecting the solution's viscosity is the polymer's molecular weight. A polymer solution with a higher molecular weight will often be more viscous than one with a lower molecular weight. One of the requirements for electrospinning, which produces fibers, is the presence of polymers with appropriate molecular weight and viscosity in the solution. The polymer solution is stretched as it travels away from the needle tip and toward the collection plate during electrospinning. As the polymer solution is stretched, entanglement between the molecule chains prevents the electrically driven jet from fragmenting, maintaining a continuous solution jet. Since the length of the polymer chain determines how much the polymer chains are entangled in the solvent, the molecular weight of the polymer corresponds to the size of the polymer chain, which in turn affects the viscosity of the solution when electrospun monomeric polymer solution does not produce fibers [54]. Increasing the polymer concentration is another way to make the solution more viscous. The jet will not break during electrospinning if the concentration increases because more polymer chains will entangle in the solution, similar to when the molecular weight increases[36].

Physical properties

Natural polymers, including chitosan, alginate, and collagen, have been examined for their physical characteristics as efficient reinforcement agents to fabricate the required composite material, especially in tissue engineering. This substance has been investigated as nano-hydroxyapatite (n-HAP), with dimensions of 15-200 nm in length and 10-80 nm in width [55, 56]. Recently, it was suggested that n-HAP could be used as an inorganic carrier for metallic-based nanocomposites in food-active packaging [57]. Furthermore, the tensile strength of collagen casting films increased when four weight percent of n-HAP was added, going from 38.98 to 48.20 MPa, and their water barrier performance doubled[32].

3.5 Relevant parameters

Flow rate

The flow rate of the solution feeding to the spinneret significantly impacts the shape of the fiber produced during a particular electrospinning process. By applying an electric field to a charged fluid droplet, electrospinning has fibers with sizes ranging from nanometers to micrometers. The Taylor cone, the initial shape of the droplet before it becomes a fiber, is formed by the solution feed to the

spinneret, and its formation is critical. The polymer in the solution feedstock may solidify inside the spinneret tip at low flow rates, making it challenging for the droplet to form into a Taylor cone. This could result in a reduction in fiber diameter or the development of beads on the fiber, which would be detrimental to the end product's quality. The solution may trickle quickly from the spinneret tip if the flow rate is too high, which can also reduce fiber diameter [43].

The impact of the solution flow rate on fiber morphology is evident within a specific range of flow rates. Any increase in the feeding rate results in an increase in the diameter of the electrospun fibers. This is because the size of the droplet generated at the spinneret tip increased with the flow rate. As a result, the diameter of the electrospun fiber rises correspondingly. Beyond a certain point, however, the increase in flow rate may also cause a decrease in fiber diameter because of the unstable Taylor cone formation. An ideal flow rate range should be identified to obtain the desired fiber morphology and prevent the development of beads or inconsistent fibers[44].

Distance

Another critical factor in determining fiber morphologies is separating the spinneret and the collector. The form of the generated fibers is influenced by the solvent evaporation rate, the jet's movement, and the distance between the spinneret and the collector. Thinner fibers can be collected by extending the reach between the spinneret and the collector. This is because traveling over a longer distance gives the solvent more time to evaporate while reducing the fiber's diameter. Extended tip-to-collector distance gives the jet more room to move, stretch, and align, potentially changing the fibers' architecture [1].

However, it should be noted that it will only occur if the working distance stays within a tolerable range. The polymer solution might not get to the collector if the distance is too far, which would reduce the amount of fiber produced. The solvent may not have enough time to evaporate if the spacing is too close, which could result in the development of beads or thicker fibers[43].

Voltage

Electrospinning is a process that occurs when a potential difference is established between a solution and a collector. When a high voltage is applied, the solution's surface becomes charged, and a jet develops as the charge density rises. The thin fiber created by stretching the charged electrospinning jet is then dropped onto a collector. The conductivity of the solution, the electric field around the electrospinning jet, and the dissipation of charges on the polymer fibers deposited on the collector all affect the electrospinning process. Because it affects the solution's capacity to transmit electrical

charges, the conductivity of the solution is crucial to the electrospinning procedure. An electrospinning jet will be more stable because a more conductive solution will enable a more substantial electric charge to be built up[18].

The electrospinning process is also influenced by the electric field that surrounds the electrospinning jet. The size and shape of the electrospinning jet, and consequently the size and morphology of the resultant fibers, are also determined by the electric field. The electric field can be altered by varying the voltage provided to the solution and the distance between the spinneret and the collector. Another significant factor influencing the electrospinning process is the dissipation of charges on the polymer fibers deposited on the collector. The electrical charge on the fibers might pile up and reject successive fibers if they are not released from them soon enough, which causes a non-uniform deposition of fibers on the collector [18].

3.6 Instruments

Spinbox

The microfiber in this experiment was produced through electrospinning with a simple, safe, and configurable device called Spinbox from the Spanish manufacturer Bioinicia Fluidnatek. The Spinbox is made for dual purposes, electrospinning or electro spraying, and is identified by production number P 20220623-P1. The instrument has three main components: the box where the fibers are produced, a syringe pump to deliver the solution stored in the syringe with a controllable flow rate and the high voltage power supply. In our case, the positive high voltage is included in the Spinbox, controlled, and monitored through a scrutable button and a display in the lower part of the box itself. In contrast, the negative voltage is added externally, which means that every time we desired to produce fibers with negative voltage, we had to use an external power supply. The instrument was delivered almost ready to use; some small particles were assembled following the instructions and an external camera was mounted, which was not included in the shipment. Finally, “WinPumpTerm” was installed, a Windows-based functioning software licensed by BIONIA from the graphical user interface to control the pump. *Figure 3-4* shows the Spinbox and syringe pump used in this thesis.

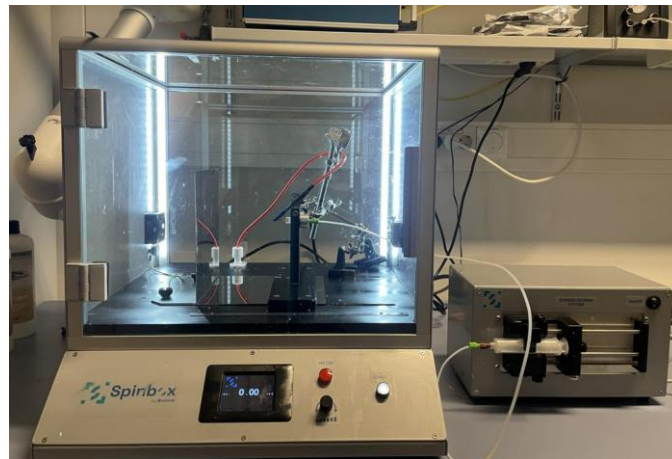


Figure 3-4. Electrospinning instrument ‘ Spinbox and syringe pump’ used for the experiment.

Pump

The pump relates to cables to the Spinbox and a PC where the pumping rates are controlled. Under production, the solution from a syringe is pumped through a tiny tube until it reaches the spinning head and jets toward the collector through the tips, also connected to the high voltage.

Collector

The Spinbox already has a conductible flat metallic collector. We used it in the first instances since and noticed that collecting fiber afterward was challenging; we preferred to cover the plate with aluminum foil, make the extraction more accessible, and friendly transportation of the fibers to the microscope lab. The idea of aluminum was adopted earlier in several other experiments, such as the effect of needle length, electrospinning distance, and solution concentration on the morphological properties of polyamide-6 electrospun nanowebs[40].

Spinning

Our experiment follows the try-and-error method to find the most favorable parameters (flow rate, emitters distance, and high Voltage) to produce fibers and achieve the requirements of nanofiber, which will be utilized for our novel product. A practical experiment was chosen to establish the relationship between nanofiber diameter and spinning parameters, and several experiments were done for the parametric study. The process itself decided the starting and ending point for the parameter by running the spinning from a lower rate until it reached the critical point. It started producing fibers and finished running when fibers were no longer made. PVP/TEOS and CA microfibers are the

primary experimental materials, and the research plan considers three parameter tests with positive and negative voltage, as shown in *Table 3-1*.

Table 3-1. Experimental plan for parameters

Polarity	Parameters		
	Flow rate [ml/hr]	Voltage [kV]	Emitter-tip distance [cm]
Positive	0.5 -2.5	6.1 - 20	4 -18
Negative	0.5 -2.5	15 – 19	4 -18

The experiment design includes 14 attempts where two variables were kept constant, and one varied. Both solutions have three attempts, each with an except for PVP (in positive voltage), the flow rate, and the voltage test have two attempts each.

4 Experimental program CA and PVP nanofibers

4.1 Nanofiber production

A quantitative analysis was conducted to optimize the electrospinning parameters (see Chapter 5) to produce nanofiber with a 100-200 nm diameter. In general, two different polymer aqueous solutions and four concentrations were selected to make the microfibers as described in *Table 4-1*. First, two polymer solutions with two different concentrations each (Type A, B, C, and D) were prepared. A and B are solutions with varying concentrations of polyvinylpyrrolidone (PVP) and Tetraethoxysilane (TEOS) as a solute and ethanol as a solvent. In comparison, Type C and Type D are two polymer solutions with different concentrations prepared from cellulose acetate and acetone as the solvent.

Table 4-1. Description of the polymer concentration used in this experiment.

Type	Solutions
A	PVP/Ethanol/TEOS [6g - 30g - 4.68g]
B	PVP/Ethanol/TEOS [1.55g - 15g - 2.34 g]
C	CA/Acetone [12.5 g -100ml]
D	CA/Acetone [12.5g - 87.5g]

Apart from the considered solution, the impact of the emitter size and the voltage, including positive and negative high voltage, were also examined, as summarized in *Table 4-2* and *Table 4-3*.

Table 4-2. Description of code adopted in the experiment with positive high voltage.

Positive Voltage	
Code	Description
PVP-A-G18-F	Test with PVP/TEOS solution type A, emitters size gauge 18 for flow rate effect.
PVP-B-G18-F	Test with PVP/TEOS solution type B, emitters size gauge 18 for flow rate effect.
PVP-A-G15-D	Test with PVP/TEOS solution type A, emitters size gauge 15 for distance effect.
PVP-A-G18-V	Test with PVP/TEOS solution type A, emitters size gauge 18 for voltage effect.
PVP-A-G18-V	Test with PVP/TEOS solution type A, emitters size gauge 18 for voltage effect.
CA-C-G15-F	Test with CA solution type C, emitters size gauge 15 for flow rate effect.
CA-D-G15-D	Test with CA solution type D, emitters size gauge 18 for distance effect.
CA-C-G15-V	Test with CA solution type A, emitters size gauge 15 for voltage effect.

Table 4-3. Description of code adopted in the experiment with negative high voltage.

Negative Voltage	
Code	Description
PVP-A-G15-F	Test with PVP/TEOS solution type A, emitters size gauge 15 for flow rate effect.
PVP-A-G15-D	Test with PVP/TEOS solution type A, emitters size gauge 15 for distance effect.
PVP-A-G15-V	Test with PVP/TEOS solution type A, emitters size gauge 15 for voltage effect.
CA-C-G15-F	Test with CA solution type C, emitters size gauge 15 for flow rate effect.
CA-C-G15-D	Test with CA solution type C, emitters size gauge 15 for distance effect.
CA-C-G15-V	Test with CA solution type C, emitters size gauge 15 for voltage effect.

4.2 Chemicals and Reagents

The chemicals and precursors used in this study are Cellulose acetate (CA) (Sigma-Aldrich, from Schnellendorf Distribution density: 1.3 g/ml), Polyvinylpyrrolidone (PVP) (Sigma-Aldrich, from Schnellendorf Distribution), Tetraethoxysilane (TEOS) (Thermo-science, purity: 99.9%, density: 0.934 g/ml), Acetone (VWR International, density: 0.792 g/ml) and Ethanol (Merck KGaA, Darmstadt Germany, density: 0.79 g/ml). All chemicals were used as received, displayed in [Figure 4-1](#) below.



Figure 4-1 Chemicals and reagents used in thesis.

4.3 PVP/TEOS

The polyvinylpyrrolidone/tetraethyl orthosilicate solution, also known as PVP/TEOS, is one of the two solutions chosen to produce the fibers, where ethanol was used as a solvent. The procedure and concentration for preparing PVP/TEOS were based on previous studies[30, 46]. The initial “type A” see [Table 4-1](#). solution was designed with the ratio adopted in the survey conducted by Frontera, P. et al. 1: 5: 0.78 per wt.%.

The electrospun fiber produced at the first trial with the considered ratio dissolved in water. This is attributed to the hydrophobic behavior of the PVP/TEOS to water. However, the adsorbing material's structural stability is crucial in adsorption systems. To overcome this challenge, TEOS was added to PVP [46]. Therefore, a second, "type B” microfiber with 150% TEOS concentrations was introduced to our experiment; the addition of the TEOS was equivalent to almost 50% in “type B” compared to “type A.” The polyvinylpyrrolidone/tetraethyl orthosilicate solution, also known as PVP/TEOS, is one of the two solutions chosen for our experiments, where ethanol is used as a solvent. The procedure and concentration for preparing PVP/TEOS were based on other studies [30, 46]. The preparation process was identical in both type A and type B solutions; TEOS/PVP (Type B) polymer solution was made of 1.55 g of PVP powder, 15 g of ethanol, and 2.34 g of TEOS in contrast to type A, which

consisted of 6g PVP, 30g ethanol and 4.68 TEOS. Both type B and type A solutions were stirred for 30 min before adding the TEOS.

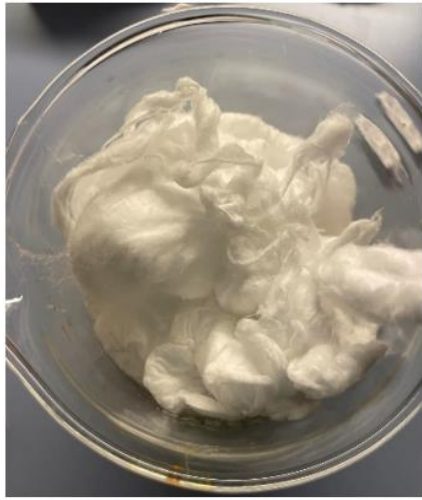


Figure 4-2. Raw electrospun microfibers



Figure 4-3. Microscopic visualization of the PVP/TEOS microfibers in water

4.4 Cellulose Acetate (CA)

The CA solution is prepared by dissolving cellulose acetate into acetone. Here also, as in PVP, an unexpected phenomenon happened. Coagulation see [Figure 4-5](#) of the solution during electrospinning was observed. Several studies [2, 33] reported coagulation in electrospinning with CA-solution. They suggested upgrading the viscosity of the solutions to decrease the coagulations, as is mentioned in the electrospun fibers properties (see section (3.4)). A new solution with a higher concentration of CA Type D was introduced. Inspired by the literature suggests, a slight improvement was observed, and the solution was jetted for a more extended period without facing coagulation see [Figure 4-4](#).

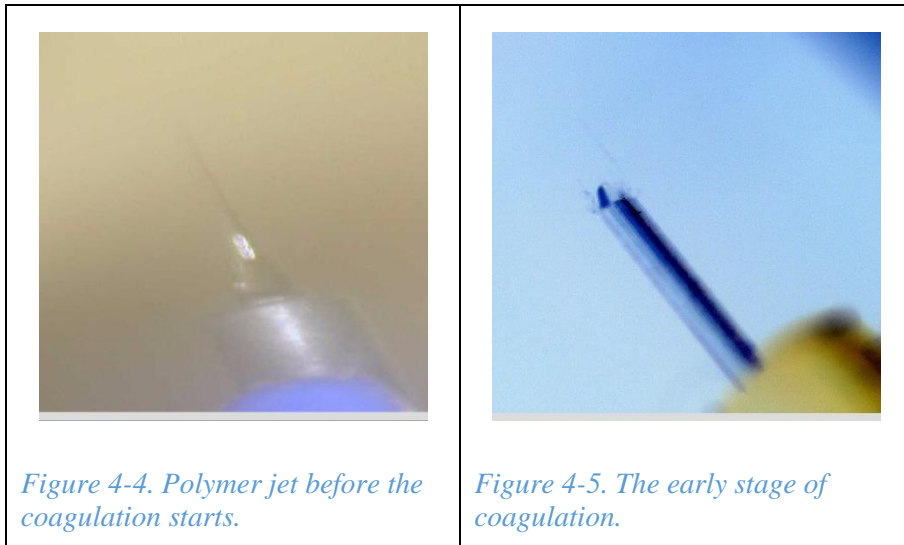


Figure 4-4. Polymer jet before the coagulation starts.

Figure 4-5. The early stage of coagulation.

4.5 Preparation of materials

The solution was prepared in the fume hood at OsloMet Chemistry laboratory in accordance with the Norwegian Health and safety standard (HMS). The chemicals were kept at room temperature, and it should be noted that all tests were conducted at the actual room temperature.

PVP/TEOS Solution

The TEOS/PVP (Type A) polymer solution was first prepared by dissolving 1 g of PVP powder in 5 g of ethanol at room temperature, stirring at around 500 rpm for 30 minutes. Then 0.78 g of TEOS was added to the solution (at room temperature), and the mixture was left stirring overnight. The TEOS/PVP (Type B) polymer solution, containing 1.55 g of PVP powder, 5 g of ethanol, and 0.78 g of TEOS, was prepared similarly to the Type A solution.

Cellulose Acetate CA

CA-solution was prepared following the work of Chousidis, N. et al [29], using Cellulose Acetate as a solute and Acetone as a solvent. For type C, 12.5 g of cellulose acetate was dissolved in 100 ml acetone and kept in a 600 ml bottle to stir overnight. The same procedure was adopted to produce CA-solution type D with a reduced acetone content (around 87.5 ml).

5 Optimization and characterization of microfiber properties

An optical microscope OLYMPUS GX71, *Figure 5-1*, was used to analyze the microstructure and morphology of the developed fibers. The device was set at 10-bit gray, and the distance was calibrated by measuring first a known object: a needle Gauge 18. The needle was measured at 717.53 μm , equivalent to its actual size, with an estimated error of 0.003 μm (see section (5.1)).

The fibers were collected in aluminum foil and put directly into the camera's optic. The light reflection made the visualization of the fibers challenging. Maneuvering different options from the microscope application and covering the top of the aluminum foil with a dark plate helped to overcome this problem slightly. A better solution couldn't be considered due to the small quantity of the produced fiber. Once a better visual focus of the manufactured fibers was achieved, pictures were taken, and parallel measurements of the diameters were recorded. A detailed description of the procedure can be found in Appendix 1. The average of 12-diameter measurements from different fibers in the same sample spot was calculated to determine the fiber size in each test. *Figure 5-1* shows the outlook of the microscope illustration, which we also used to measure the diameter size.



Figure 5-1. Optical microscope OLYMPUS GX71

5.1 Measurement Error

A stainless-steel syringe tip, gage 22, with an outer diameter of 0.72 mm *Figure 5-3*, was utilized to check the microscope's precision for the diameter measurement. The object had known dimensions from the standard. It was set in focus first so that the visualization was comfortable enough and measured the tube's outer diameters. As a result, the outer tube diameter was measured at 717,53 μm *Figure 5-2* and *Figure 5-4* equivalent to 0.71753 mm. The correspondent error would then be the difference between the actual standard size and the measured one, corresponding to 0.00247.

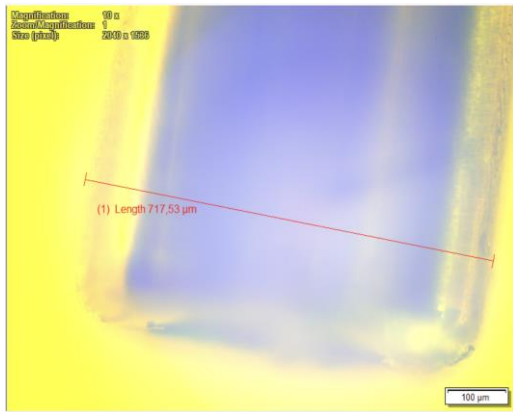


Figure 5-2. Measurement for the outer diameter

PRECISION STAINLESS STEEL TIPS									
Gauge	Color		ID		OD		6.35 mm (0.25")	12.7 mm (0.50")	
			mm	inch	mm	inch			
14	Olive		1.54	0.060	1.83	0.072	7018029	7018043	
15	Amber		1.36	0.053	1.65	0.065	–	7018068	
18	Green		0.84	0.033	1.27	0.050	7018107	7018122	
20	Pink		0.61	0.024	0.91	0.036	7018163	7018178	
21	Purple		0.51	0.020	0.62	0.032	7005005	7018233	
22	Blue		0.41	0.016	0.72	0.028	7018260	7018272	
23	Orange		0.33	0.013	0.65	0.025	7018302	7018314	
25	Red		0.25	0.010	0.52	0.020	7018333	7018345	
27	Clear		0.20	0.008	0.42	0.016	7018395	7006008	
30	Lavender		0.15	0.006	0.31	0.012	7018424	7018433	
32	Yellow		0.10	0.004	0.24	0.009	7018462	–	

Figure 5-3. Actual standard size for gauges in the market.

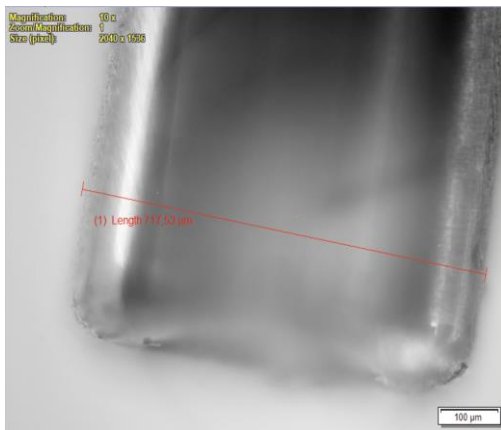


Figure 5-4. Measurement for the outer diameter



Figure 5-5. Illustration of gauge 22

5.2 PVP/TEOS Fiber with positive voltage application

5.2.1 Flow rate effect

In this session are presented the result of the PVP/TEOS microfiber experiment in the form of a chart. The investigation aimed to check the effect of flow rate in electrospinning with emitter size gauge 18 and PVP/TEOS type A and B solution. The voltage and the emitter's distance were kept constant while the flow rate ranged from the lowest when fibers started to be produced to the highest possible rate until the jets started to lose their stability. According to the study of the process optimization and modeling of electrospun cellulose acetate nanofibers, the second-order polynomial was used to determine the correlation of the models [39].

PVP/TEOS -A-G18-F

The PVP/TEOS -type A (6g PVP - 30g Ethanol – 4.68g TEOS) - with emitter size Guage 18 – flow rate effect conducted in this experiment results are presented as a model in the chart *Figure 5-6*.

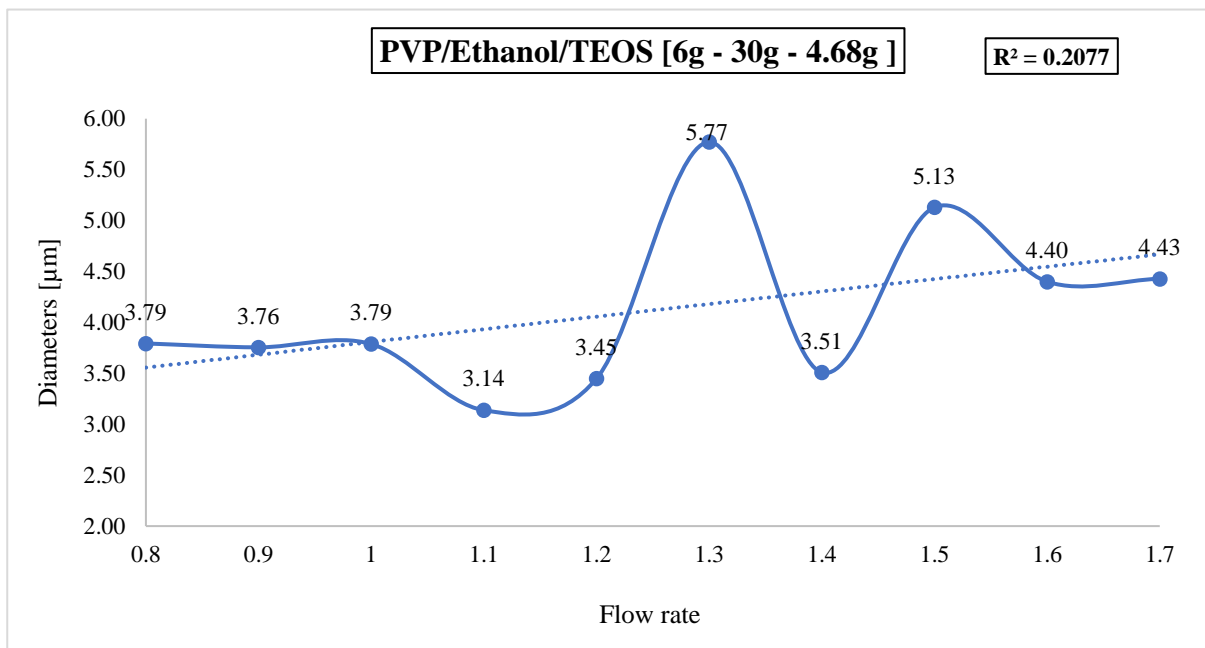


Figure 5-6. Microfibers made of PVP/Ethanol/TEOS [6g - 30g - 4.60g] diameter illustration chart.

In this case, the diameter of the fibers by the flow rate between 0.8 and 1.7 [ml/hr.] fluctuated with slight variations between the size of 3.17 [μm] to 2.9 [μm]. The trend starts to change, starting from 0.1 ml/hr Until ca. 1 ml/hr with a constant diameter, and begins to decrease at a flow rate of 1 ml/hr until it reaches the minimum diameter at flow range 1.1 – 1.2 ml/hr.

The Flow rate effect test ranges from 0.8 to 1.7 ml/hr, indicating the significance of the model fit. The efficiency can be described by the regression coefficient of $R^2=0.2077$, which suggests that the model generally has a poor correlation. However, a partially strong correlation is shown if it considers the 1-1.3 ml/hr ranges and 1.3-1.5 ml/hr. In our case, PVP/TEOS will not be examined further; otherwise, the flow rate range of 1.1- 1.2 ml/hr is a promising parameter for optimizing our product.

PVP-B-G18-F

The PVP/TEOS -type B (1.55g PVP - 15g Ethanol - 2.34g TEOS) - with emitter size Guage 18 – flow rate effect conducted in this experiment results are presented as a model in the chart *Figure 5-7*.

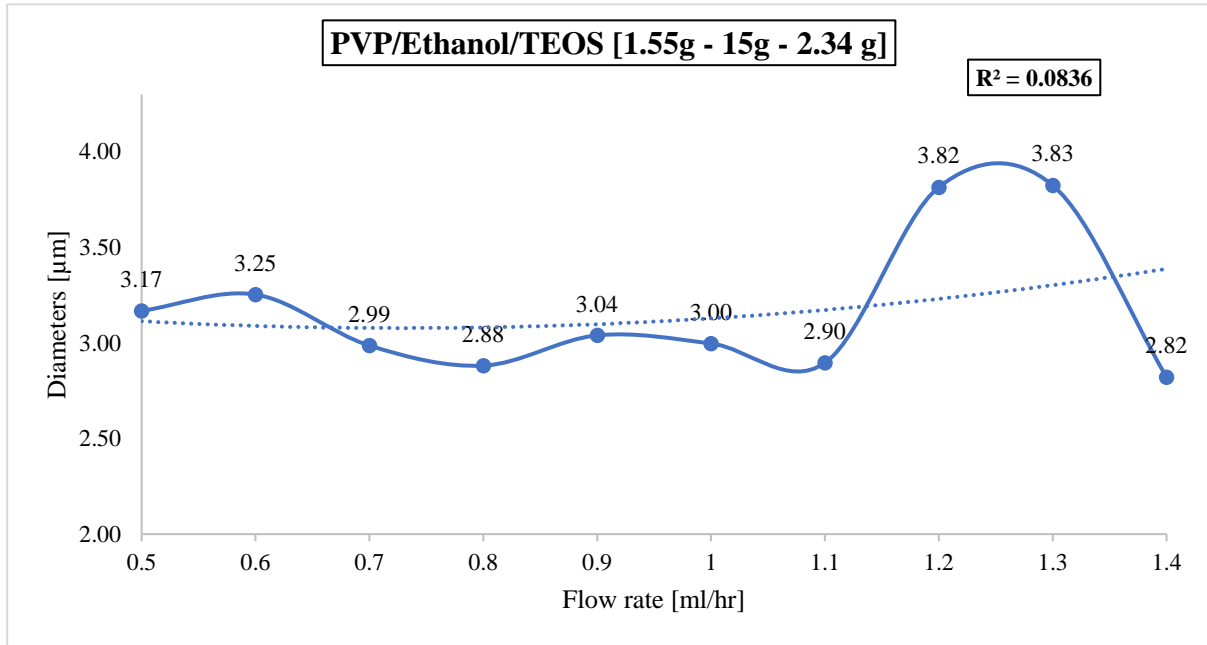


Figure 5-7. Microfibers made of PVP/Ethanol/TEOS [1.55g - 15g - 2.34 g] diameter illustration chart.

In this case, the diameter of the fibers produced by the flow rate is between 0.5 and 1.1 [ml/hr.] have a slight variation between the size of 3.17 [µm] to 2.9 [µm]. It starts from 1.1 ml/hr. until ca. 1.25 appear to change in trend by increasing the diameter from 2.9 [µm] to almost 4 [µm] and collapsing again to 2.82 [µm] at 1.4 ml/hr.

The Flow rate effect test ranges from 0.8 to 1.7 ml/hr. indicates the significance of the model fit, and the model's efficiency is revealed by the regression coefficient of $R^2 = 0.0836$, which suggests that the model generally has an extremely poor correlation. However, a partially strong correlation is shown if it is considered the ranges between 1.1-1.4 ml/hr. In our case, PVP/TEOS will not be examined further; otherwise, the flow rate range is 1.1- 12 ml/hr. would be considered a promising parameter for the optimization of our product.

5.2.2 Distance effect

In this session are presented the result of the PVP/TEOS microfiber experiment will be in the form of a chart. The experiment aimed at checking the effect of the distance of the emitter tip to a collector in electrospinning with emitter size gauge 15 and PVP/TEOS (type A) solution. The Voltage and the Flow rate were kept constant while the distance varied from the lowest to the highest critical values possible. According to Electrospinning Setup and Procedure study, the second-order polynomial can satisfy the correlation between the diameter [64].

PVP-A-G15-D

The PVP/TEOS -type A (3g PVP - 15g Ethanol - 2.34g TEOS) - with emitter size Guage 15 – emitter tip to the collector effect conducted in this experiment results are presented as a model in the chart *Figure 5-8*.

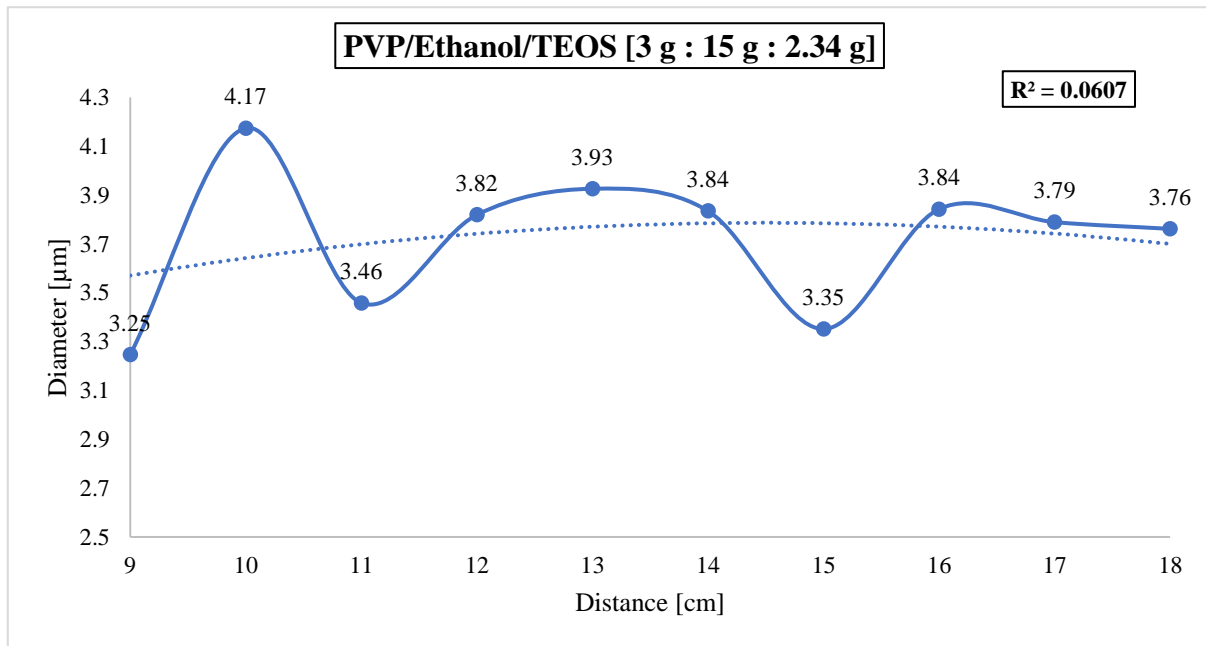


Figure 5-8. Microfibers made of PVP/Ethanol/TEOS 3 g : 15 g : 2.34 g diameter illustration chart.

In this case, the fibers' diameter is produced by gradually altering the distance of the emitter from 9 cm to 18 cm. The diameter rises until its highest value is 4.17 μm at 10 cm. Because the stretching distance between the tip-to-collector distance increased, the diameter of the fiber decreases slowly up to 3.46 μm at 11 cm [37]. Then the trend gets a more constant frequency, and the diameter of the fibers varies between 3.46 to 3.84 until the process reaches its highest distance of 18 cm.

The model in *Figure 5-8* behavior can be described as a polynomial function and gives a regression value of $R^2=0.0607$, which is a poor correlation through the whole range. However, a partially strong correlation is shown if it considers the 9-11, 11-15, and 14-16 cm range partly in the 9-11 11-15 cm field, which could be a range of interest.

The relationship between the diameter and the distance in the 9 to 10 cm range appears proportional while inversely proportionate in the 10 to 11 cm range. The same trend appears in the field of 11 to 15 cm with a turning point at the distance of 13 cm, whereas the length between 11-10 and 13-15 cm could be considered promising ranges for our research to achieve a small diameter size.

5.2.3 Voltage effect

In this session are presented the result of the PVP/TEOS microfiber experiment in the form of a chart. The investigation aimed to check the effect of voltage in electrospinning with emitter size gage 18 and PVP/TEOS type A. The Flow rate and the emitter's distance were kept constant while the voltage starts from the fibers began to be produced at the highest possible speed, where the jets started to lose instability. According to the theoretical trend line in a study [64], the voltage versus diameter graph is predicted as a polynomial function, which is also adopted in this session to determine the standard deviation and the regression value.

PVP-A-G18-V

The PVP/TEOS -type A (3g PVP - 15g Ethanol - 2.34g TEOS) - with emitter size Guage 18 – flow rate effect conducted in this experiment results are presented as a model in the chart [Figure 5-9](#).

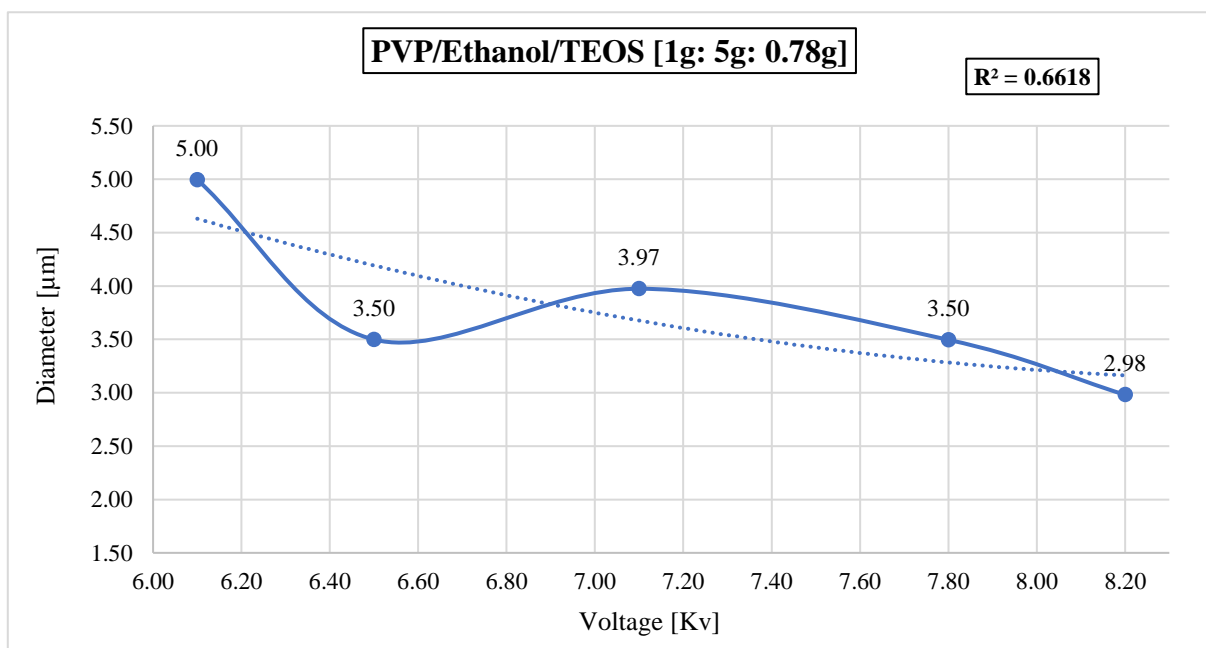


Figure 5-9. Microfibers made of PVP/Ethanol/TEOS [1g: 5g: 0.78g] diameter illustration chart.

In this case, the fibers are produced by changing the voltage from 6.10 kV to 8.10 kV. This trial was the first one for our experiment, and it was helpful in a way that enriched our ability to sort the outcome of the spinning wisely later. The graph in [Figure 5-9](#) shows a decrease in fiber diameter since the first round until it reaches the smallest size of 3.5 µm at 6.5 kV and increases again up to 3.97 at 7.10 kV. Further performance shows that the diameter decreases to the highest voltage of 8.2 kV and reaches its smallest size of 2.98 µm.

The model behavior can be described as a polynomial function and gives a regression value of $R^2=0.6618$, a better correlation than the previous experiments. However, a partially strong correlation is shown if it considers the ranges between 6.1-7.1 kV and 7.1-8.2, which also fits the theory in the study [64], which discovered that increasing voltage reduced fiber diameters to a minimum before the trend reversed with further voltage increase. In contrast, studies have shown that a higher voltage initially may increase fiber diameter, but after a specific voltage, the fiber diameter begins to decrease due to further stretching of the solution droplet with higher voltage; the higher voltage may also cause faster acceleration into the collector due to the increased potential difference, resulting in less flight time for the jet to stretch before deposition.

PVP-A-G18-V

The PVP/TEOS -type A (1g PVP - 5g Ethanol – 0.78g TEOS) - with emitter size Guage 18 – flow rate effect conducted in this experiment results are presented as a model in the chart *Figure 5-10*.

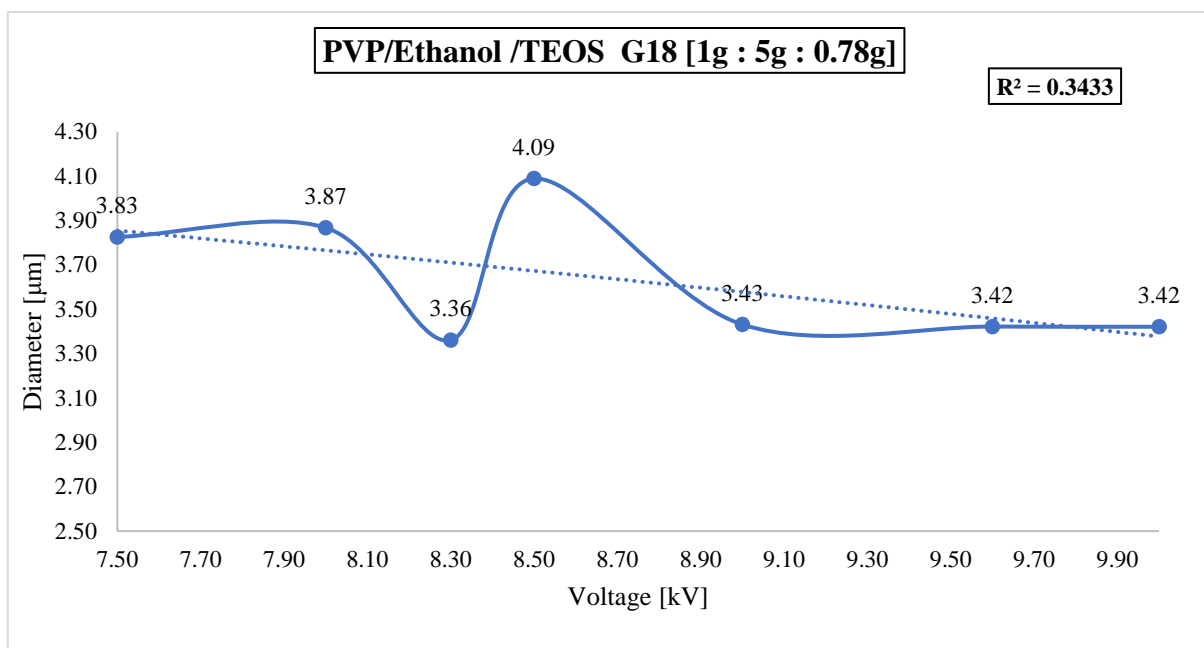


Figure 5-10. Microfibers made of PVP/Ethanol/TEOS G18 [1g: 5g: 0.78g] diameter illustration chart.

The model starts at 7.5 kV; the value of the diameters is almost equal to the previous trial and starts to increase until 8.0 kV, then turns to decrease by reaching the lowest diameter at the voltage range of 8.00 and 8.5 kV. After an instance of up and down, the diameter tends to be constant, starting from 9.0 to 10 kV.

The study [64] discovered that increasing voltage reduced fiber diameters to a minimum before the trend reversed with further voltage increase. In contrast, other studies have shown that a higher

voltage initially increases fiber diameter, but after a specific voltage, the fiber diameter decreases. In our case, the voltage-diameter model has a correlation value of R^2 0.3433, which is poor, but the range 8.0-8.5 kV and 8.3-8.90 kV have a strong correlation in partial, and it fits the theory in [64].

5.3 CA Fibers with positive voltage application

5.3.1 Flow rate effect

CA-C-G15-F

The Cellulose acetate CA -type C (12.5g CA – 100ml Acetone) - with emitter size Guage 15 – flow rate effect conducted in this experiment results are presented as a model in the chart *Figure 5-11*. The voltage and the emitter's distance were kept constant while the flow rate varied from the lowest to the highest possible. According to the study of the process optimization and modeling of electrospun cellulose acetate nanofibers [39], the correlation of the model is determined by the second-order polynomial.

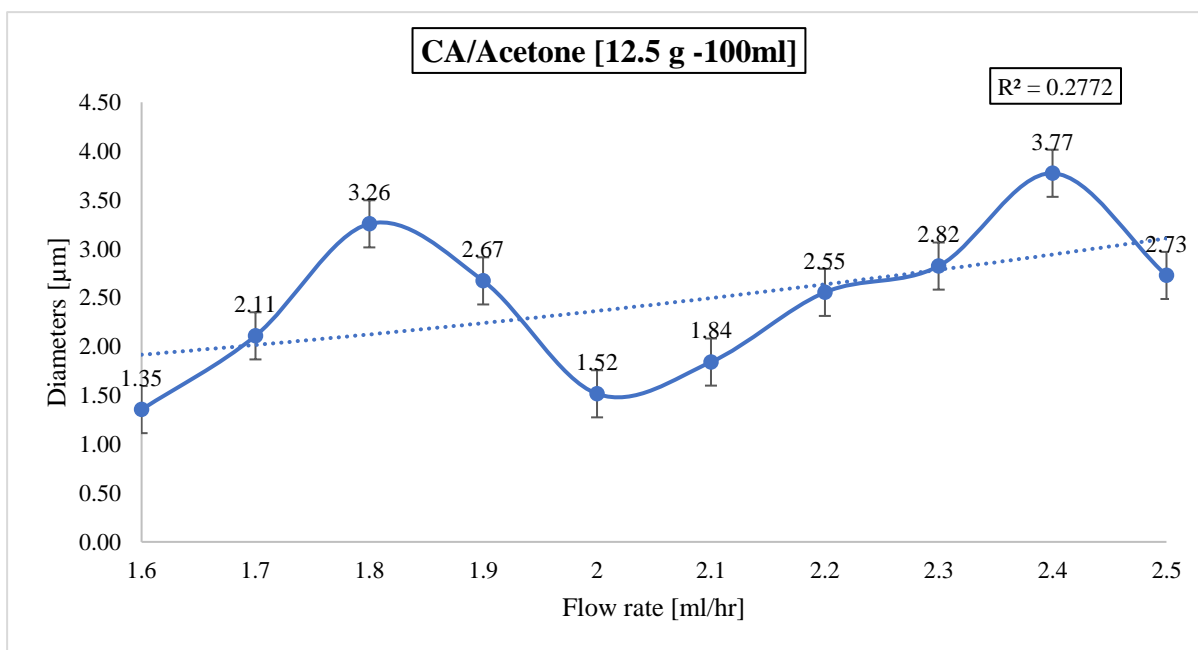


Figure 5-11. Microfibers made of CA/ Acetate [12.5 g -100ml] diameter illustration chart.

The graph shows that the diameters size of the fibers is relatively smaller regarding the flow effect in the fibers produced by the PVP/TEOS. Even though the introduction of a higher pumping rate, the trend tends to fluctuate with a similar frequency throughout the model. The model starts with a smaller diameter for the fiber at 1.6 ml/hr, followed by the trend increasing until the pump reaches 1.8 ml/hr flow rate and decreases until it reaches 1.52 µm fiber diameter at 2 ml/hr flow rate.

The Flow rate effect test ranges from 1.6 to 2.5 ml/hr, indicating the significance of the model fit, and the model's efficiency is revealed by the coefficient of the correlation $R^2 = 0.2772$, which suggests that the model only explains a poor correlation of the in the whole model in general. However, a partially strong correlation is shown if it considers the ranges between 1.6-2.0 ml/hr and 2.3-2.5 ml/hr.

5.3.2 Distance effect

CA-D-G15-D

The Cellulose Acetate CA -type D (12g CA – 87.5ml) - with emitter size Guage 15 – emitter tip to the collector effect conducted in this experiment results are presented as a model in the chart *Figure 5-12*. This test aimed to check the impact of the distance between the emitter tip to the collector in electrospinning. The Flow rate and voltage were kept constant while the flow rate varied from the lowest to the highest possible. The fiber diameter may decrease as the stretching distance increases between the tip and the collector. Therefore the correlation of the model is determined as a second-order polynomial based on studies [39].

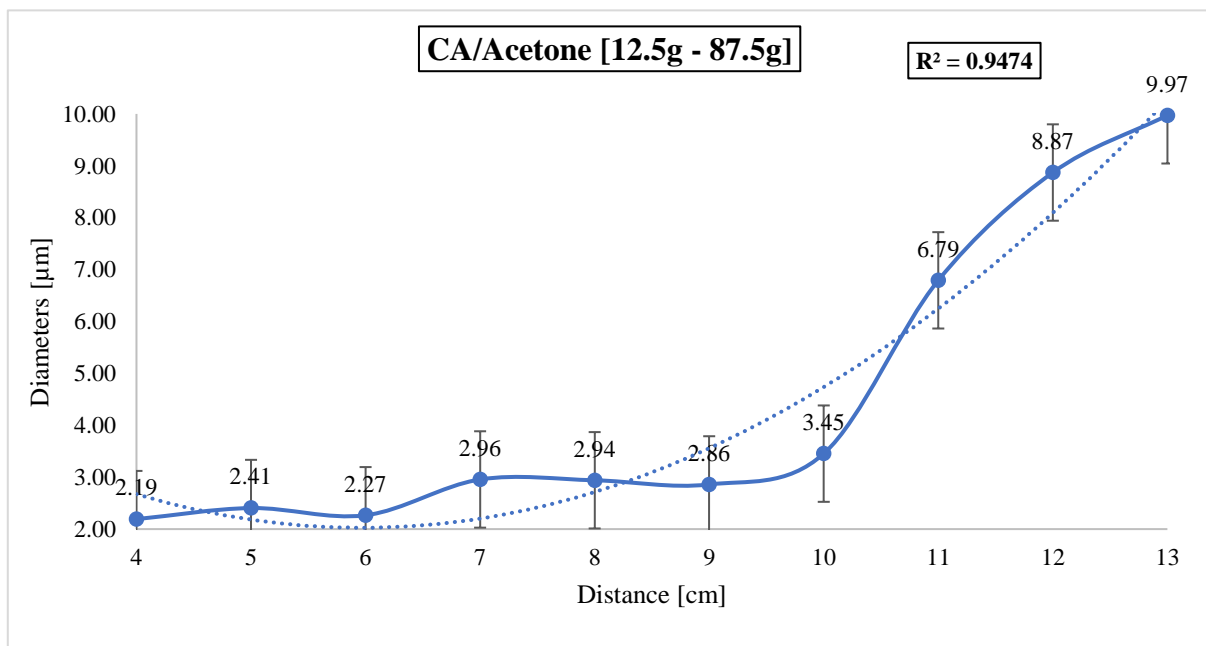


Figure 5-12. Microfibers made of CA/ Acetate [12.5g - 87.5g] diameter illustration chart.

Here the trend is quite different and looks like the phenomena for nanofiber manufacturing “The less the distance of the emitter from the collector, the less the diameter of the fibers” [40]. Therefore, by moving the emitter from the nearest to the farthest distance, manufacture fiber with bigger and bigger diameters. Thus, the model in *Figure 5-12* behavior can be described as a polynomial function with a regression value of $R^2 0.9474$, which shows a strong correlation. According to the Electrospinning

Setup and Procedure study, when the voltage is kept constant while the distance is varied, the electrospinning jet behavior and collected fiber profile are similar to when the voltage is varied. At the same time, the tip-to-collector distance is kept constant [64].

5.3.3 Voltage effect

CA-D-G15-V

The Cellulose Acetate CA -type D (12.5g CA – 87.5ml Acetone) - with emitter size Guage 15 – voltage effect conducted in this experiment results are presented as a model in the chart *Figure 5-13*. This test aimed to check the effect of voltage in electrospinning, where the Flow rate and the emitter's distance were kept constant. In contrast, the voltage from the fibers started to be produced at 15.5 kV to the highest possible speed, 20 kV, where the jets started to lose instability. According to the theoretical trend line in the study [64], the voltage versus diameter graph is predicted as a polynomial function, which is also adopted in this session to determine the standard deviation and the regression value. According to the theoretical trend line in the study [64], the voltage versus diameter graph is predicted as a polynomial function, which is also adopted in this session to determine the standard deviation and the regression value.

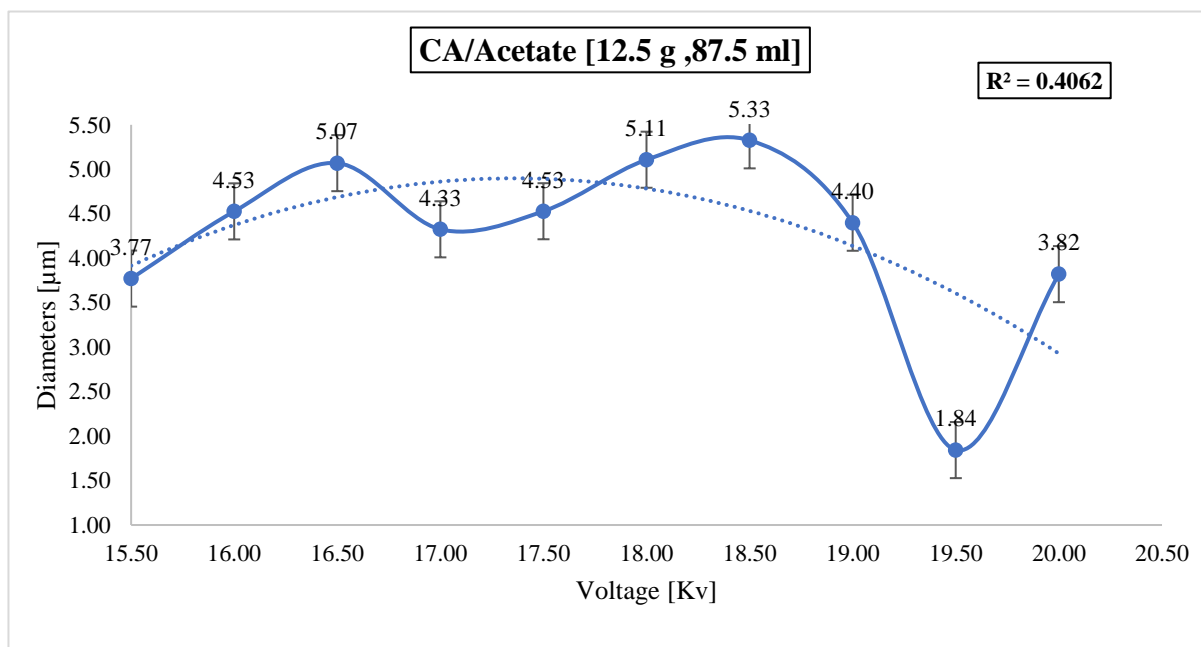


Figure 5-13. Microfibers made of CA/Acetate [12.5 g, 87.5 ml] diameter illustration chart.

In this case, the graph in *Figure 5-13* shows an increase in diameter from the starting voltage up to 16.5 kV, continuing with a certain instability until it reaches 18.5 kV. The model becomes a polynomial curve where the lowest voltage at 19.5 kV gives the smallest fiber size, 1.84 µm. The

voltage versus diameter in this session could be predicted as a polynomial function with a standard deviation of R^2 0.4062, which is not strong enough. However, the range 19-20 kV has a strong correlation and could be determined as a range of interest.

5.4 PVP/TEOS Fibers with negative voltage application

5.4.1 Flow rate effect

PVP/TEOS-A-G15-F

The PVP/TEOS -type A (6g PVP - 30g Ethanol – 4.68g TEOS) - with emitter size Guage 15 – flow rate effect conducted in this experiment results are presented as a model in the chart *Figure 5-14*. The negative voltage and the emitter's distance were kept constant while the flow rate ranged from 0.8 ml/hr when fibers started to be produced to the highest possible rate, 1.7 ml/hr, where the jets started to lose instability. The goal is to determine the effect of flow rate in the electrospinning process; therefore, fibers were processed by keeping the voltage and emitter’s distance constant. The second-order polynomial determines the correlation of the model in this session *Figure 5-14* according to the study of the process optimization and modeling of electrospun cellulose acetate nanofibers [39].

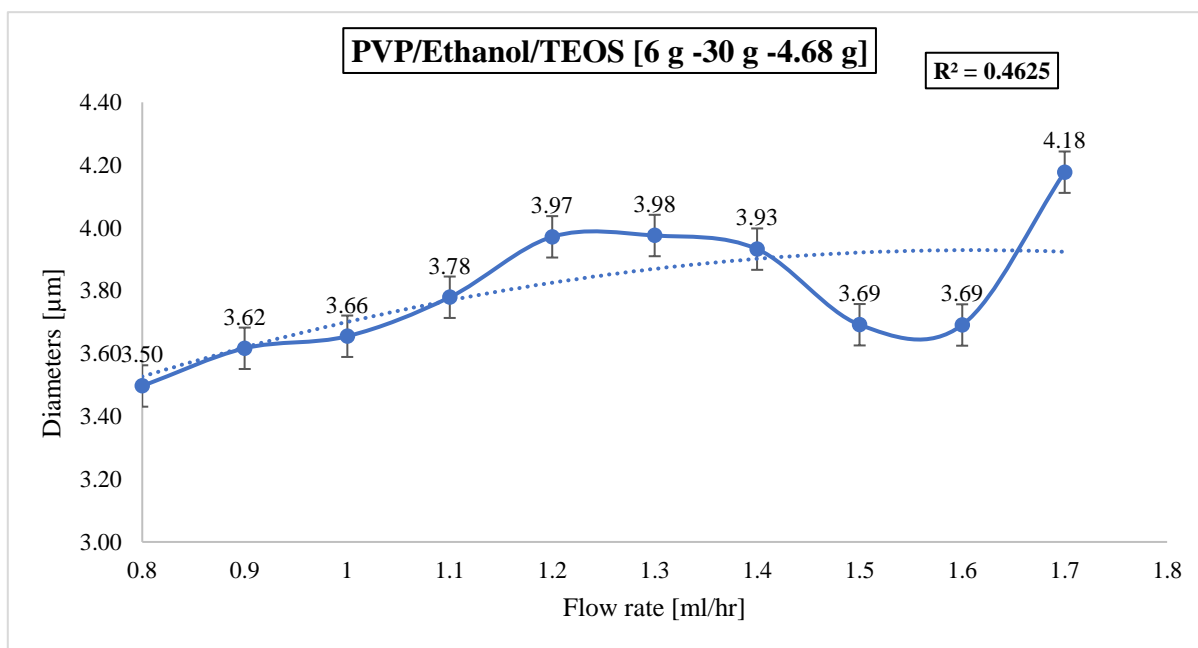


Figure 5-14. Microfibers made of PVP/Ethanol/TEOS [3 g -15 g -2.34 g] diameter illustration chart.

The Flow rate effect test ranges from 0.8 to 1.7 ml/hr, indicates the significance of the model fit, and the model’s efficiency is revealed by the coefficient of the correlation ($R^2 = 0.4625$), which suggests that the model has no strong correlation.

5.4.2 Distance effect

PVP/TEOS-A-G15-D

The PVP/TEOS -type A (6g PVP - 30g Ethanol – 4.68g TEOS) - with emitter size Guage 15 – distance effect conducted in this experiment results are presented as a model in the chart *Figure 5-15*. This test aimed to check the impact of the distance between the emitter and the collector in electrospinning. The flow rate and negative voltage were kept constant while the distance moved from the lowest of 9 cm to the highest possible of 18 cm, where the jet stopped reaching the collector. According to the Electrospinning Setup and Procedure study, the second-order polynomial can satisfy the correlation between the diameter and the diameter [64].

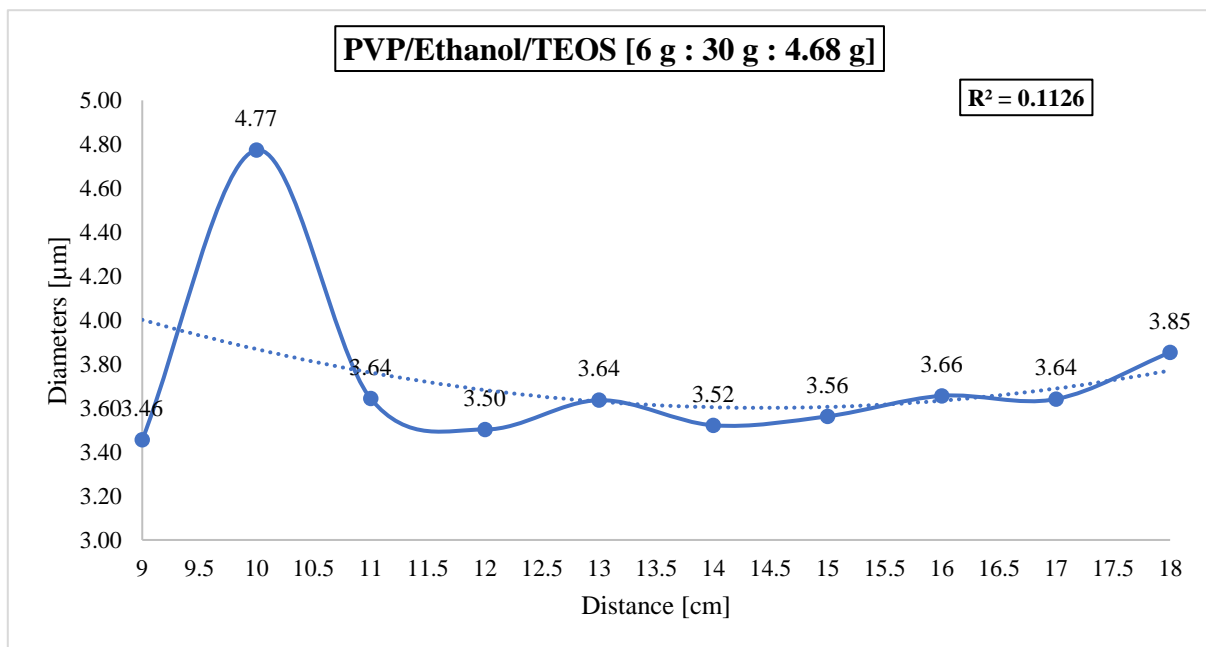


Figure 5-15. PVP/Ethanol/TEOS [3 g : 15 g : 2.34 g]

When the voltage is kept constant, the electrical field's magnitude is proportional to the distance in the opposite direction. The spread in a typical electrospinning setup ranges from 10 to 15 cm, generally allowing enough flight time for the solvent to vaporize and deposit a dry fibers strand [37]. In our case, the strength of the electric field is slightly inversely proportional to the distance in the range of 10 cm to 15 cm. The model in *Figure 5-15* behavior can be described as a polynomial function that gives a regression value of $R^2=0.1126$, which is not such a strong correlation. Still, in the 9-11 cm range, the correlation is stronger enough to count as a range of interest.

5.4.3 Voltage effect

PVP/TEOS-A-G15-V

The PVP/TEOS -type A (6g PVP - 30g Ethanol – 4.68g TEOS) - with emitter size Guage 15 – voltage effect conducted in this experiment results are presented as a model in the chart *Figure 5-16*. The distance and the flow rate were kept constant while the negative voltage varied from the lowest of 9 kV to the highest possible 13.5, where the jet started to lose their instability. According to the Electrospinning Setup and Procedure study, the voltage is kept constant while the distance varies. The electrospinning jet behavior and collected fiber profile are like those when the voltage changes. At the same time, the tip-to-collector distance is kept constant [64].

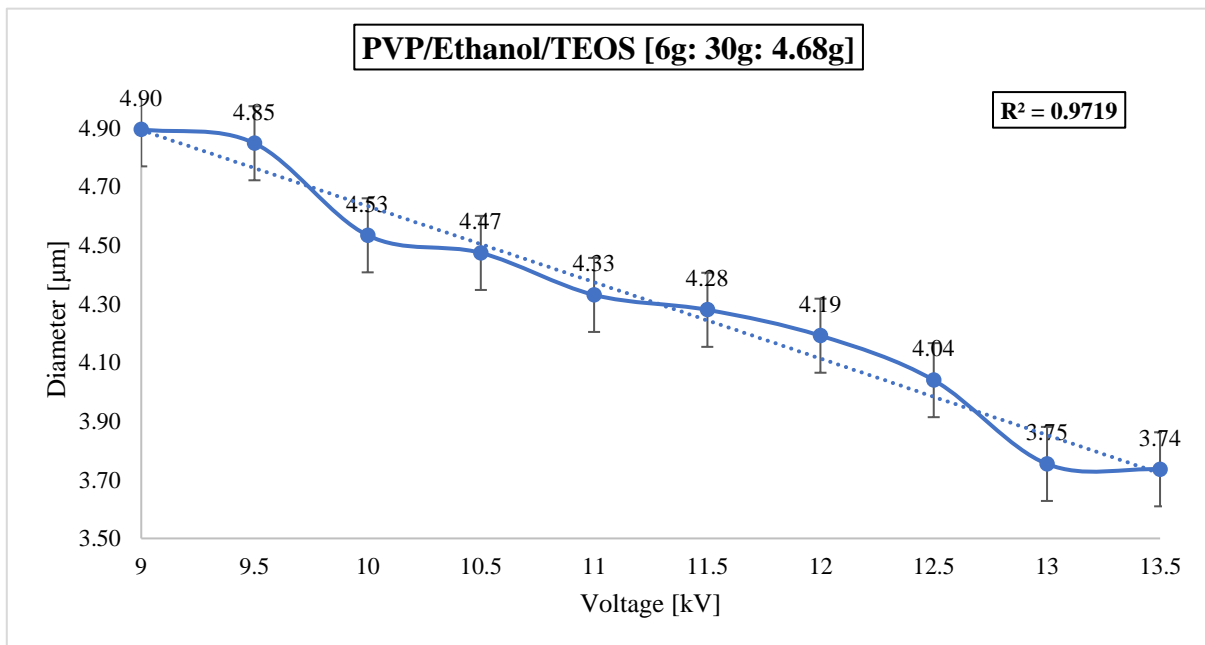


Figure 5-16. PVP/Ethanol/TEOS [1g: 5g: 0.78g]

In this case, the model in *Figure 5-16* shows that the diameter of the fiber kept decreasing while the voltage increased until it reached the minor diameter, 3.74 μm at 13.5kV. The trend here partially fits the [37] theory, which discovered that increasing voltage reduced fiber diameters to a minimum before the trend reversed with further voltage increase. The trend line for model voltage versus diameter in this session could be predicted as a polynomial function with a standard deviation of R^2 0.9719, which is a strong correlation and makes the range permissible for our research.

5.5 CA Fibers with negative voltage application

5.5.1 Flow rate effect

CA-C-G15-F

The Cellulose acetate CA -type C (12.5g CA – 100ml Acetone) - with emitter size Guage 15 – flow rate effect conducted in this experiment results are presented as a model in the chart *Figure 5-17*. The negative voltage and the emitter's distance were kept constant while the flow rate varied from the lowest of 5 ml/hr to the highest possible 5.9 ml/hr, where the emitter started dripping. The second-order polynomial determines the correlation of the model in this session *Figure 5-17* according to the study of the process optimization and modeling of electrospun cellulose acetate nanofibers [39].

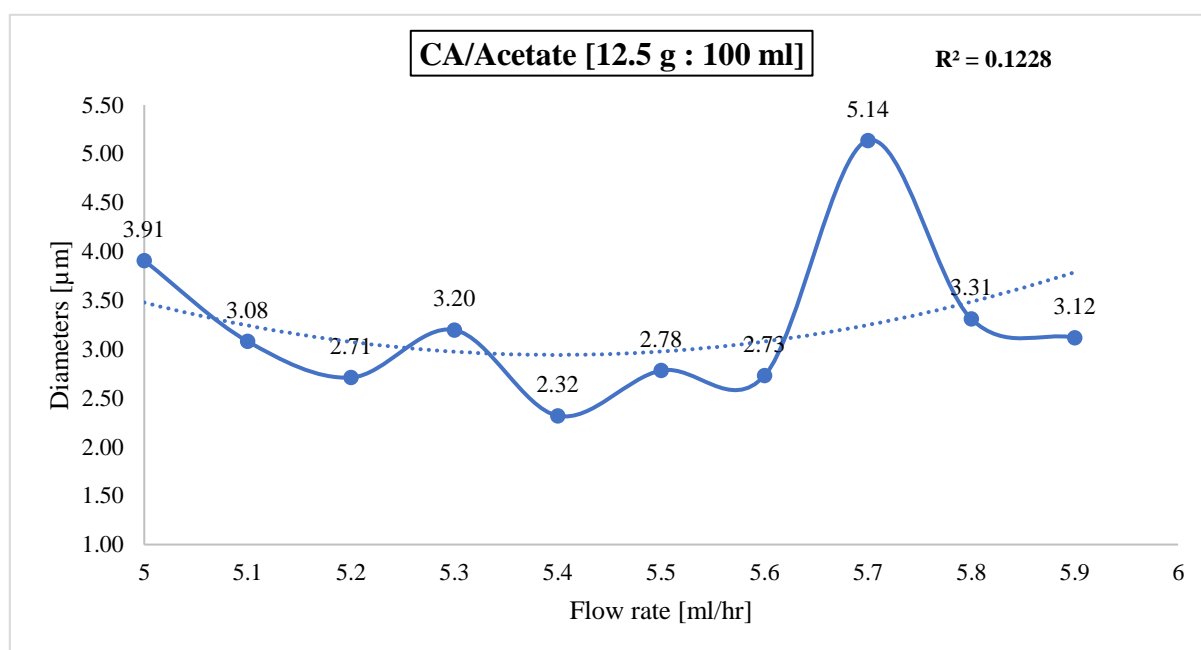


Figure 5-17. Microfibers of CA/Acetate [12.5 g: 100 ml] diameter illustration chart.

The Flow rate effect test ranges from 5 to 6 ml/hr, shows the significance of the model fit, and the model's efficiency is revealed by the coefficient of the correlation $R^2 = 0.11228$, which indicates that the model does not have a strong correlation in general, but the range 5.2-5.4 ml/hr and 5.6-5.8 ml/hr have a strong correlation and could be determined as a range of interest.

5.5.2 Distance effect

CA-C-G15-D

The Cellulose Acetate CA -type D (12.5g CA – 100ml Acetone) - with emitter size Guage 15 – emitter tip to the collector effect conducted in this experiment results are presented as a model in the chart

Figure 5-18. This test aimed to check the impact of the distance between the emitter and the collector in electrospinning. The Flow rate and negative voltage were kept constant while the distance varied from the lowest of 4 cm to the highest possible of 13 cm, where the jets started to lose their stability. The fiber diameter may decrease as the stretching distance increases between the tip and the collector; therefore, the correlation of the model is determined as a second-order polynomial based on studies [39].

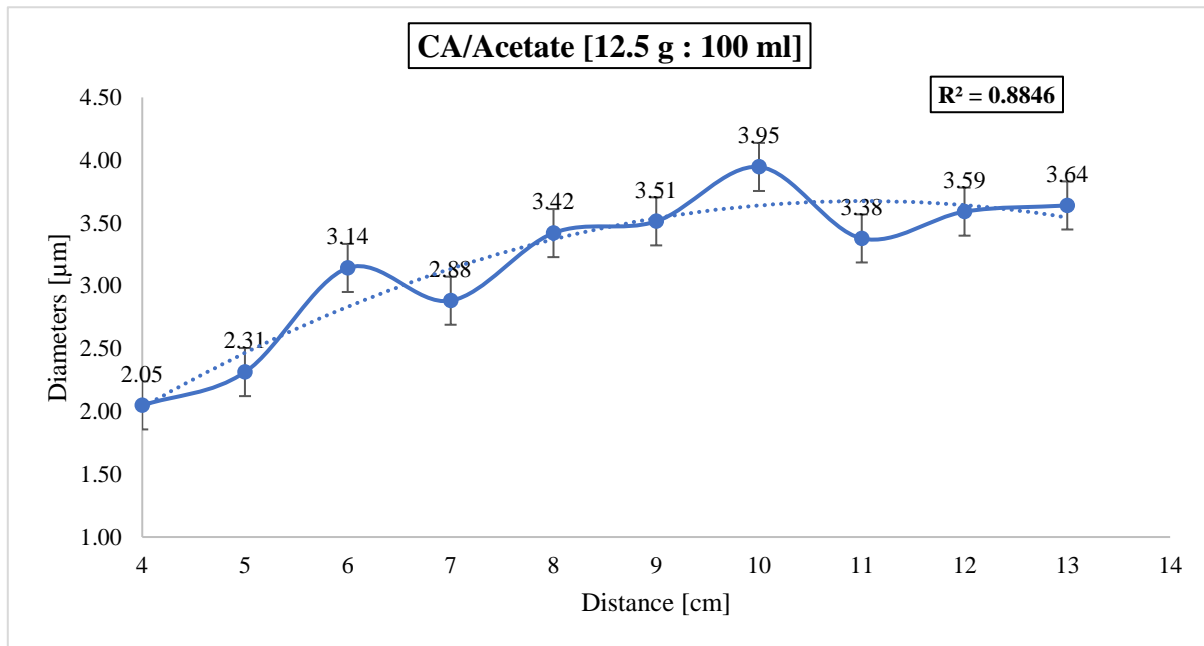


Figure 5-18. Microfibers made of CA/Acetate [12.5 g : 100 ml] diameter illustration chart.

According to our research, If the voltage is kept static, the electrical field's magnitude is proportional to the distance in the opposite direction. The distance in a typical electrospinning setup ranges from 10 to 15 cm, generally allowing enough flight time for the solvent to vaporize and deposit a dry fiber strand [37].

In our case, the strength of the electric field is slightly inversely proportional to the distance in the range of 10 cm to 15 cm. Therefore, the graph *Figure 5-18* behavior can be described as a polynomial function with a regression value of $R^2=0.8846$, which is a far better correlation than the previous one.

5.5.3 Voltage effect

CA-C-G15-V

The Cellulose Acetate CA -type D (12.5g CA – 100ml Acetone) - with emitter size Guage 15 – voltage effect conducted in this experiment results are presented as a model in the chart *Figure 5-19*. This test aimed to check the effect of voltage in electrospinning, where the flow rate and the emitter's

distance were kept constant. In contrast, the voltage ranged from the lowest to the highest possible speed, where the jets started to lose instability. According to the theoretical trend line in the study [64], the voltage versus diameter graph is predicted as a polynomial function, which is also adopted in this session to determine the standard deviation and the regression value.

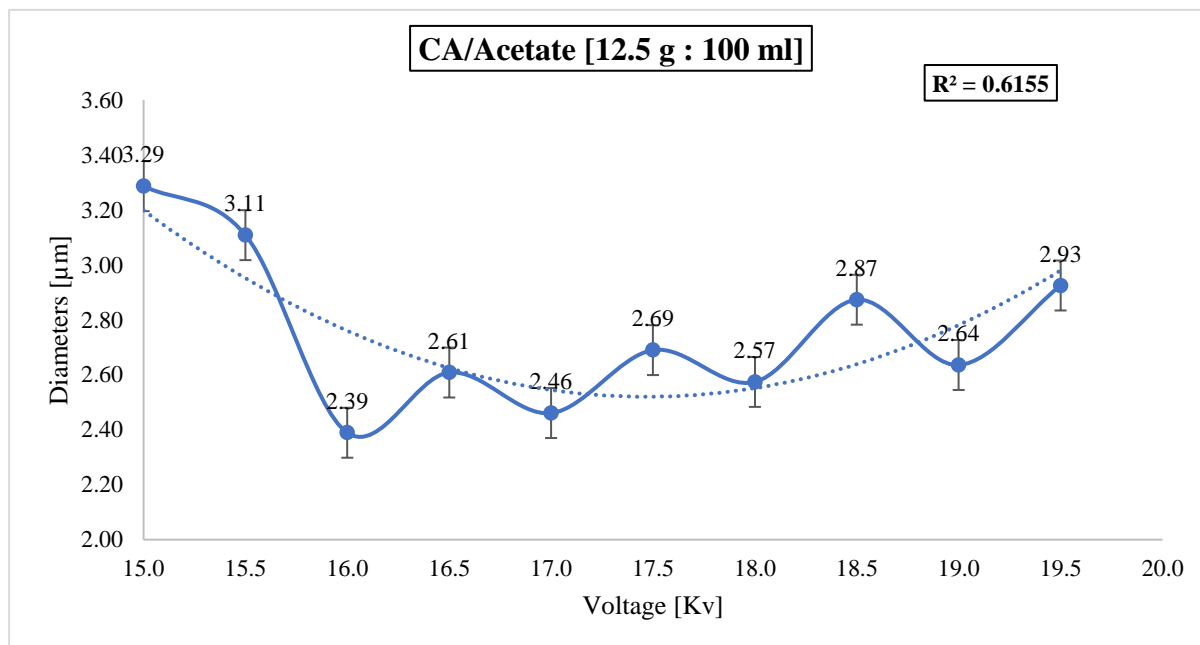


Figure 5-19. Microfibers made of CA/Acetate [12.5 g : 100 ml] diameter illustration chart.

In this case, *Figure 5-19*, the model starts with a descending trend at the lower voltage and increases with increasing voltage. Increasing voltage reduced fiber diameters to a minimum before the trend reversed with further voltage increase [37]. According to the theoretical trend line [64], the voltage-diameter graph in this session could be predicted as a polynomial function with a standard deviation of R^2 0.6155, which is a low correlation that the previous PVP/TEO, but a symmetrical trend is shown in the flow and creates five partially substantial polynomial deviations every time the voltage increases of two kV.

6 Microfiber Optimization result

The quantitative research for Electrospun microfibers production led our research to understand better the impact of the parameters, which have considerable importance in guiding the further process for producing fibers with a minor diameter size. The effect of the solution's concentration on the fiber's workability and morphology was also a central subject. Besides, the PVP/TEOS microfiber produced shows weak resistance to water, which switches our original plant and excludes PVP/TEOS microfiber as a second reinforcing material for the mechanically reinforced cementitious material. At the same time, the exploring for the parameter considers both PVP/TEOS and CA solutions. This chapter will demonstrate the experiment for optimization of the most promising parameters to produce microfiber.

6.1.1 Flow Rate Effect

The result of the flow rate effect in microfiber production with the positive voltage between the PVP and CA nanofibers is presented in *Table 6-1* and *Table 6-2*. At the same time, the graph demonstrated the correlation between the flow rate and the variation of the diameter in both materials. The CA type C in grey color in the chart shows the best result for our goal, with minimal diameters of CA microfibers and reaching the lists diameter of 1.35 μm at a flow rate of 1.6 ml/hr.

Table 6-1. Flow rate effect with the positive voltage for the PVP/TEOS and CA microfibers

Flow rate [ml/hr.]		Flow rate [ml/hr.]		Flow rate [ml/hr.]	
CA-C-G15-F		PVP-B-G18-F		PVP-A-G18-F	
Flow rate [ml/hr.]	Diameter [μm]	Flow rate [ml/hr.]	Diameter [μm]	Flow rate [ml/hr.]	Diameter [μm]
1.6	1.35	0.5	3.17	0.8	3.79
1.7	2.11	0.6	3.25	0.9	3.76
1.8	3.26	0.7	2.99	1	3.79
1.9	2.67	0.8	2.88	1.1	3.14
2	1.52	0.9	3.04	1.2	3.45
2.1	1.84	1	3	1.3	5.77
2.2	2.55	1.1	2.9	1.4	3.51
2.3	2.82	1.2	3.82	1.5	5.13
2.4	3.77	1.3	3.83	1.6	4.4
2.5	2.73	1.4	2.82	1.7	4.43

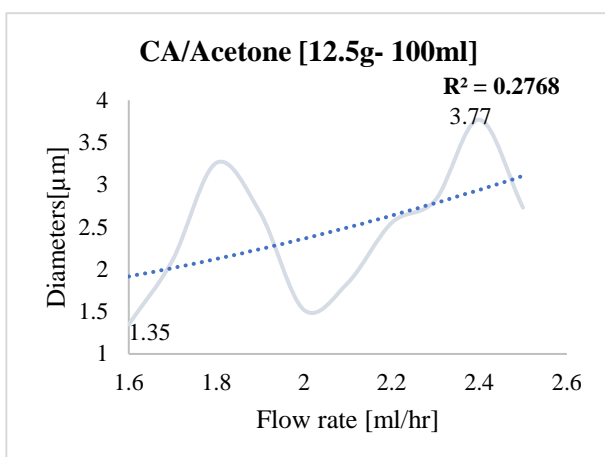


Figure 6-1. Result from CA -C-G15-F

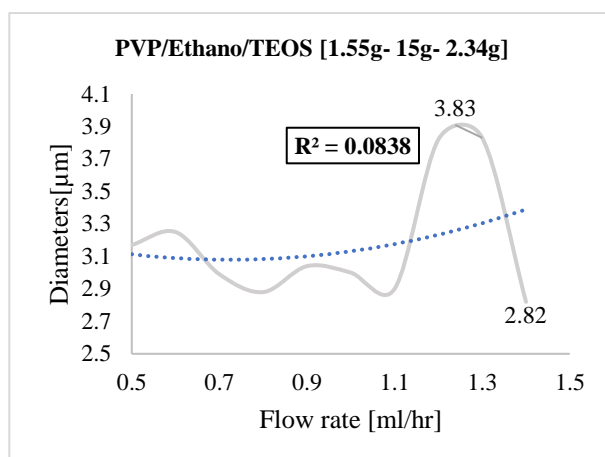


Figure 6-2. Result from PVP/TEOS -B-G18-F

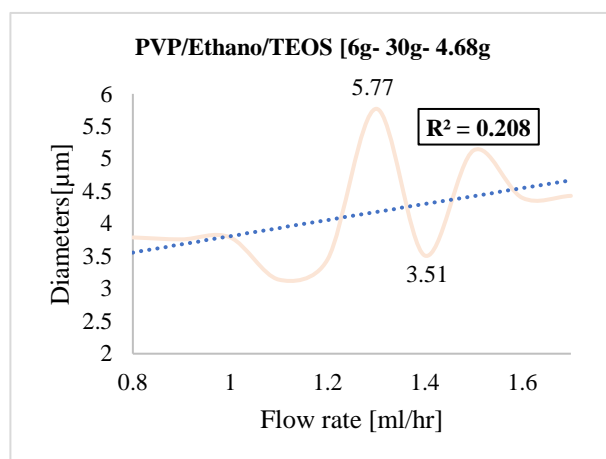


Figure 6-3. Result from PVP/TEOS -A-G18-F

Similar phenomena appear with the negative polarity, but the flow rate was increased to 5.4 ml/hr this time with an equivalent diameter of 2.32 μm , the smallest nanofiber from both materials.

Table 6-2. Flow rate effect with negative voltage for PVP/TEOS and CA microfiber

Flow rate [ml/hr.]			
PVP-A-G15-F		CA-C-G15-F	
Flow rate [ml/hr.]	Diameter [μm]	Flow rate [ml/hr.]	Diameter [μm]
0.8	3.50	5	3.91
0.9	3.62	5.1	3.08
1	3.66	5.2	2.71
1.1	3.78	5.3	3.20
1.2	3.97	5.4	2.32
1.3	3.98	5.5	2.78
1.4	3.93	5.6	2.73
1.5	3.69	5.7	5.14
1.6	3.69	5.8	3.31
1.7	4.18	5.9	3.12

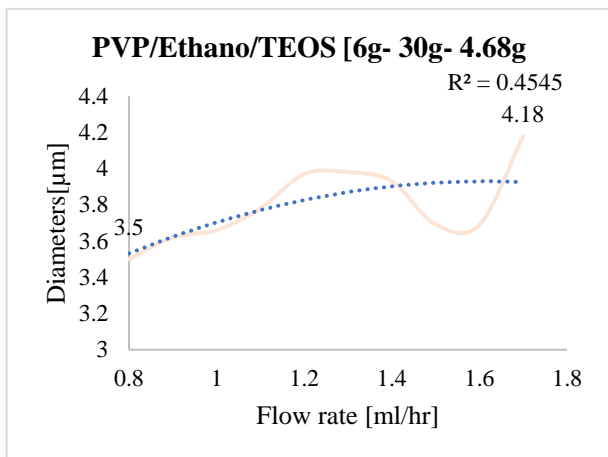


Figure 6-5. The result for the Flow rate effect PVP-A-G15-F

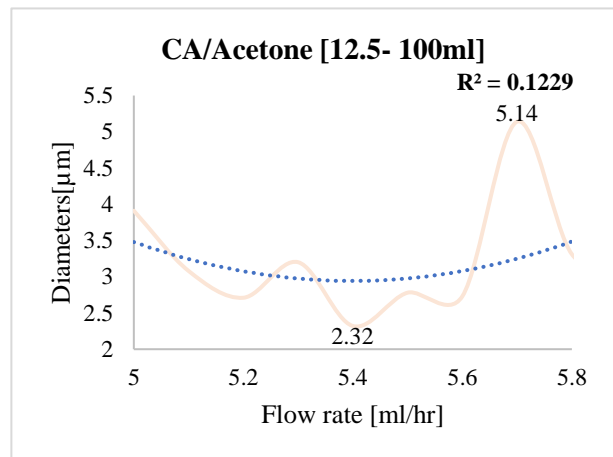


Figure 6-4. Result for the Flow rate effect CA-C-G15-F

6.1.2 Emitters Distance Effect

The result of the emitter’s tip-to-collector distance effect in nanofiber production with the positive voltage between the PVP and CA nanofibers is presented in *Table 6-3* and *Table 6-4*. At the same time, the graph demonstrated the correlation between the flow rate and the variation of the diameter in both materials. The chart’s CA type D in orange color shows the best result for our goal, with a minimum diameter of CA microfibers and reaching the list’s diameter of 2.19 µm at 4 cm.

Table 6-3. The tip-to-collector distance effect with Positive voltage for PVP/TEOS and CA microfiber

Distance [cm]			
PVP-A-G15-D		CA-D-G15-D	
Distance [cm]	Diameter [µm]	Distance [cm]	Diameter [µm]
9	3.2	4	2.19
10	4.2	5	2.41
11	3.5	6	2.27
12	3.8	7	2.96
13	3.9	8	2.94
14	3.8	9	2.86
15	3.4	10	3.45
16	3.8	11	6.79
17	3.8	12	8.87
18	3.8	13	9.97

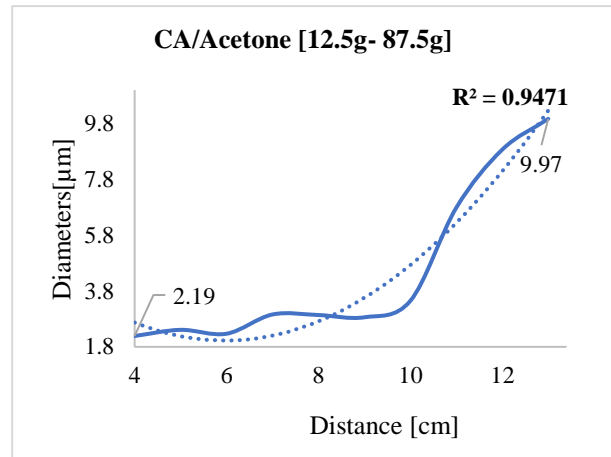
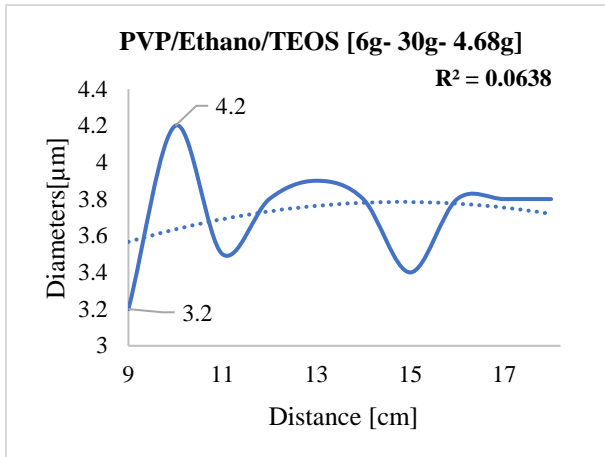


Figure 6-7. Result for distance effect PVP-A-G15-D

Figure 6-6. Result for distance effect CA-D-G15-D

A similar trend has been kept in the test with the negative polarity where the minor diameter, 2.05 μm , is registered at 4 cm from the same material.

Table 6-4. The tip-to-collector distance effect with negative voltage for PVP/TEOS and CA microfiber

Distance [cm]			
PVP-A-G15-D		CA-C-G15-D	
Distance [cm]	Diameter [μm]	Distance [cm]	Diameter [μm]
9	3.46	4	2.05
10	4.77	5	2.31
11	3.64	6	3.14
12	3.50	7	2.88
13	3.64	8	3.42
14	3.52	9	3.51
15	3.56	10	3.95
16	3.66	11	3.38
17	3.64	12	3.59
18	3.85	13	3.64

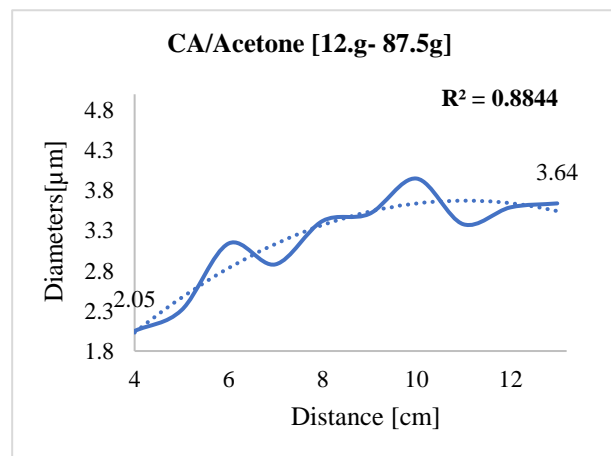
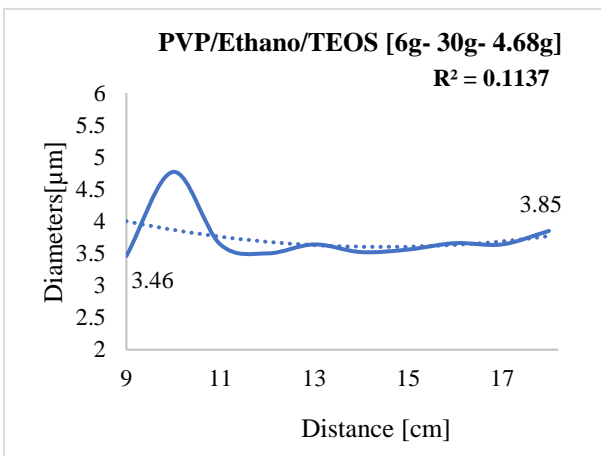


Figure 6-9. Result for distance PVP-A-G15-D

Figure 6-8. Result for distance CA-C-G15-D

6.1.3 Voltage effect

The result of the high voltage effect in nanofiber production with the positive voltage between the PVP and CA nanofibers is presented in *Table 6-5* and *Table 6-6*. At the same time, the graph demonstrated the correlation between the high voltage and the variation of the diameter in both materials. The CA type C presented in grey color in the chart shows the best result for our goal, with minimal diameters size of fibers and reaching the lists diameter of 1.84 μm at a voltage of +19.5 kV.

Table 6-5. The positive-voltage effect in PVP/TEOS and CA microfiber

Voltage [kV]					
CA-C-G15-V		PVP-A-G18-V		PVP-B-G18-V	
Voltage [kV]	Diameter [μm]	Voltage [kV]	Diameter [μm]	Voltage [kV]	Diameter [μm]
15.50	3.77	6.10	5.00	7.50	3.83
16	4.53	6.50	3.50	8	3.87
16.5	5.07	7.10	3.97	8.3	3.36
17	4.33	7.80	3.50	8.5	4.09
17.5	4.53	8.20	2.98	9	3.43
18	5.11			9.6	3.42
18.5	5.33			10	3.42
19	4.40				
19.5	1.84				
20	3.82				

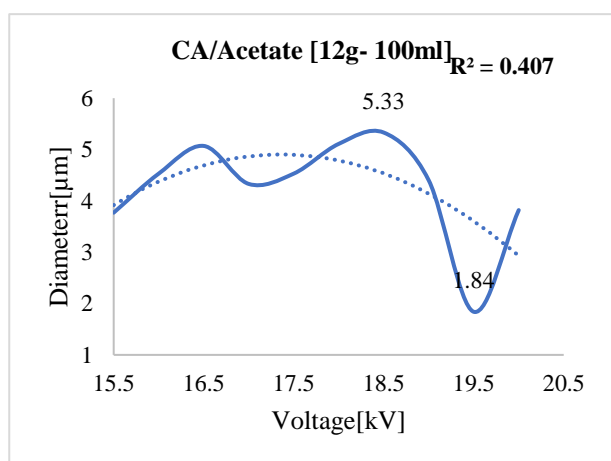


Figure 6-10 Result for the Voltage effect CA-C-G15-V

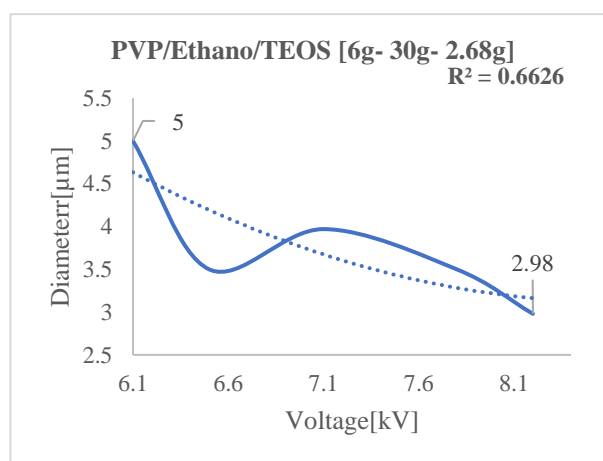


Figure 6-11. Result for the voltage effect PVP-A-G18-V

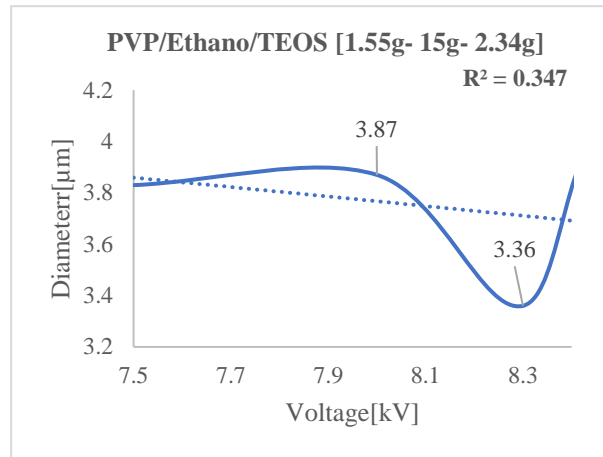


Figure 6-12. Result for the voltage effect PVP-B-G18-V

Here also the same number -19.5 kV, with negative charge produced fiber with a minor diameter of 2.93 μm.

Table 6-6. The tip-to-collector distance effect with negative voltage for PVP/TEOS and CA microfiber

Voltage [kV]			
PVP-A-G15-V		CA-C-G15-V	
Voltage [kV]	Diameter [μm]	Voltage [kV]	Diameter [μm]
-9	4.90	-15.0	3.29
-9.5	4.85	-15.5	3.11
-10	4.53	-16.0	2.39
-10.5	4.47	-16.5	2.61
-11	4.33	-17.0	2.46
-11.5	4.28	-17.5	2.69
-12	4.19	-18.0	2.57
-12.5	4.04	-18.5	2.87
-13	3.75	-19.0	2.64
-13.5	3.74	-19.5	2.93

The aim of producing nanofiber with the minor diameter possible has yet to be achieved. The results show that the fiber's average diameter is micro size. However, for this experiment, the most promising solution to manufacture the list files looks to be CA/acetone (12.5g and 100ml) with emitter size gage 15; no matter the change in voltage and the distance of the emitter, the diameter of the fiber remains relatively small.

Although the desired diameter was not achieved, the project needed to proceed; therefore, selecting the parameters and materials, which gave the smallest fiber possible, according to the diagrams, was the final step of our experiment. The most permissible parameters, in this case, were the following in [Table 6-7](#). A check-up test was run to ensure the previous test result was reasonable. The process was

the same and consisted of manufacturing fibers adopting the chosen parameters to be configured through a microscope and examining the diameter of the fiber threads by taking an average of 12 measurements from a different spot.

Table 6-7. Most promising parameters for the research

Material type	Flow rate [ml/hr.]	Voltage [kV]	Distance [cm]	Diameters [μm]
CA-C-G15-F 1.6_10_15	1.6	15	10	<u>2.27</u>
CA-C-G15-F 5.4_10_-15	5.40	-15	10	3.16
CA-C-G15-V 1.0_7_19.5	1	19.5	7	2.95
CA-C-G15-V 5.9_10_-16	5.9	-16	10	3.44

According to our experimental research, cellulose acetate with a solute concentration of 12.5 g and 100ml acetate gave the list diameter size for the nanofibers. Therefore, our novel fibers for the mechanical enhancement of the cementitious material will be manufactured using the following parameters: 1.6 ml/hr flow rate, 15 kV high voltage, and 10 cm distance between emitter and collector.

7 Cementitious composite

7.1 Materials and Sample preparation

The cement-CA electrospun microfiber composite material adopted in this experiment was an industry-grade binder known as "CEM I 52.5 R" from Heidelberg Material AS (NORCEM), a well-known Norwegian company. This binder has an excellent early-stage compressive strength of 52.5 MPa and meets NS-EN 197-1 standard Appendix 2. During the mixing process, cement was mixed with non-distilled water to add a viscose gel; then, microfibers were added.

7.2 Sample preparation

The size of the specimen (cube and prism) in compressive and tensile strength tests for cement might change depending on the precise testing needs. Whereas prism specimens used in tensile strength testing are usually 40mm x 40mm x 160 mm, cube specimens used in compressive strength tests are typically 50 mm or 100 mm on each side, according to the Norwegian Standard NS-EN 196-1:2016. Several articles [58, 67] performed the compressive strength test on different sizes of specimens. Therefore, our experiment also introduced a new measurement for the specimen. Thus, the molds and the samples used in this thesis are presented in *Figure 7-1*.

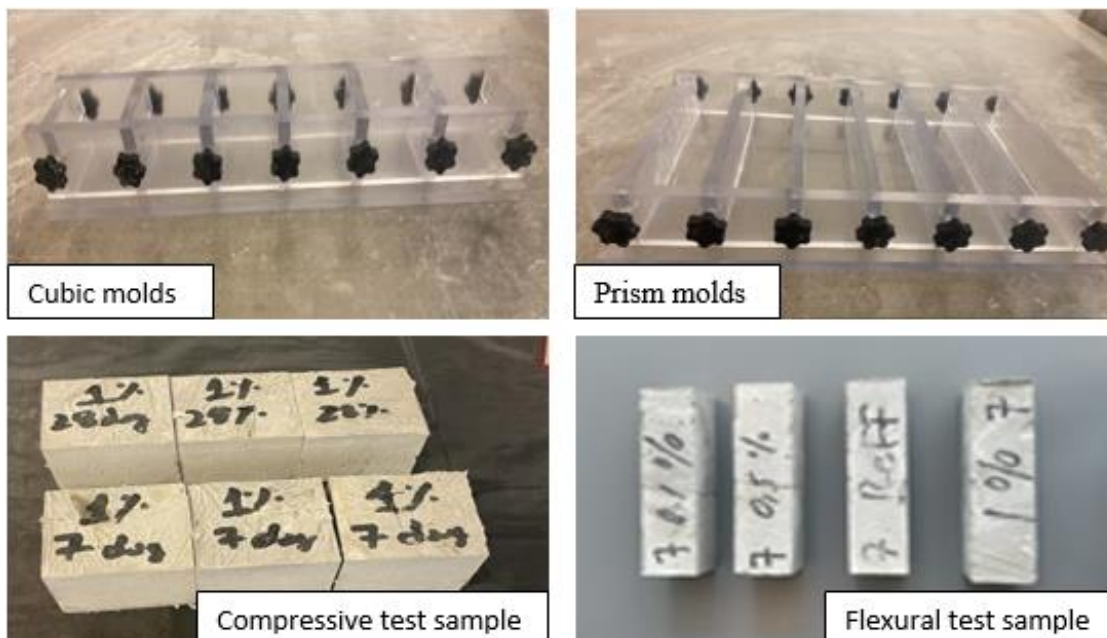


Figure 7-1. Molds and Samples used in this experiment

Admixture

As described above, the microfibers were immersed after preparing the cement paste. Unfortunately, we ran into issues with the bonding of the two materials. As seen in Figure 0.5, this resulted in an uneven distribution of electrospun particles. The observed outcomes needed to meet our initial expectations.



Figure 7-2. Admixture Cement/Microfiber demonstration

Casting and curing regime.

Several steps engage in casting and curing the cement, water, and nanofiber mix, as the Norwegian standard NS-EN 196-1:2016 describes. The ingredients are thoroughly combined, using the experimental ratio and method to ensure consistency and quality. After that, the mixture is poured into a mold and cured for 24 hours. Following this initial curing period, the mold is removed, and the specimen is immersed in water to heal for seven days for the compressive test and 28 days for the flexural test specified by the standard. This procedure ensures that the cement mixture reaches its maximum strength and durability, allowing it to be used in construction and other applications [71]. The authors prepare high-quality specimens for their thesis by following these procedures, resulting in reliable and reproducible results.

7.3 Test Methods

7.3.1 Compression strength test

The compressive strength of the cubic samples was measured using FORM+Test DELTA 5-200 machine at a constant loading rate of 2.2500 kN/s until failure. Eq. 7.1 was used to calculate the compressive strength based on the recorded values. The test was carried out in triplicates, and only the average will be presented in the following.



Figure 7-3. Compression testing machine

The compressive strength is calculated by using Eq. 7.1

$$F = \frac{P}{A} \text{ [MPa]} \quad 7.1$$

where:

- F= Compressive strength of the specimen [MPa].
- P= Maximum load applied to the specimen [N].
- A= Cross-sectional area of the specimen [mm²]

7.3.2 Flexural strength test

The flexural strength was conducted following ASTM C1609 (Standard Test Method for Flexural Performance of Fiber-Reinforced Concrete) Using Galdabini Quasar 100 machine at a constant 1 mm/min loading rate.

The sample with simple support is loaded at its center using a loading head, and the support points are positioned at equal distances from the center of the beam. Two displacement transducers spaced apart by a minimum of three times the depth of the beam were used to measure the deflection of the beam. The flexural strength of the fiber-reinforced concrete was calculated using Eq. Eq. 7.2:

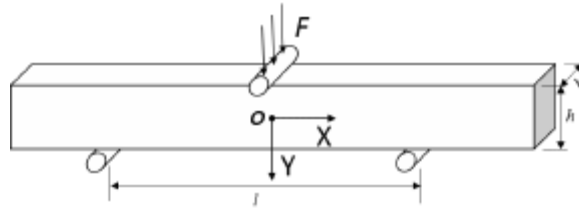


Figure 7-4. Illustration for the flexural strengths testing process.

$$f_R = \frac{3PL}{3bd^2} \quad \text{Eq. 7.2}$$

Where:

- f_R is the flexural strength of concrete.
- P is the maximum load applied to the beam
- L is the span length of the beam between the support points
- b is the width of the beam, and d is the depth of the beam

It is important to note that this formula was primarily developed for large beams. As a result, the reliability of the flexural strength results in this project could be questionable when using small beams. Small beams were initially considered due to the limitation of fiber content production. However, studies have shown an increase in strength when using small samples compared to bigger size with the same mixture [72].

8 Results and Discussions

8.1 Cellulose Acetate (CA) Microfiber

Spinnability

The spinning dopes' electro-spinnability was assessed visually and through electronic microscope pictures. In preliminary experiments, the dopes that could not electrospun were those whose mass concentrations were outside the range of 9 to 15 (% w/v). For example, spinning dopes with a CA concentration under 9 (% w/v) could not produce a continuous jet. On the other hand, a CA concentration above 15 (% w/v) was also unsuitable for electrospinning because of its high viscosity, which, when paired with the rapid rate of acetone evaporation, caused the needle tip to tight too quickly and prevented fiber creation from taking place.

There has been some controversy regarding producing CA fibers using acetone as the primary solvent. CA in solitary acetone could not create continuous fibers, according to Liu and Hsieh, and Tungprapa [47, 48]. Both studies recommended using a different solvent to help CA nanofibers form. Liu and Hsieh suggest the addition of DMAc, which is further researched by Tungprapa [47, 48].

Tungprapa argued that the higher dielectric constants and boiling point of DMAc than those of acetone are why mixed solvent systems were found to be superior in fiber formation compared to acetone as a sole solvent [48]. Acetone has also been successfully combined with acetic acid [59], N, N-dimethylacetamide [60], and dichloromethane [49] to produce other effective mixed solvents. These co-solvents are less volatile than acetone due to their higher boiling temperatures and lower vapor pressure.

Studies argued that acetone could produce a continuous jet as a single solvent, contradicting Liu, Hsieh, and Tungprapa [48, 65]. They claimed in their study that the produced nanofibers were gathered before the needle clogged [65]. One of the factors contributing to the inability to form fibers in the current study's CA concentrations beyond the evaporation acetone was the variable amounts of blockage that occurred with each run. To prevent viscous fluid buildup and enhance fiber production and collection, the needle tip for this study required regular cleaning throughout runs.

Diameter

The measured fiber diameters are in (Chapter 6), along with their values and charts. The microfibers created in this work have average sizes that range from 1.35 to 9.97 μm . Wide variations in fiber diameter are typical in electrospinning, mainly when using volatile solvents, although few studies have offered a workable solution. Significant variances in fiber sizes were typically not an issue in

wet electrospinning compared to dry electrospinning since the solvent was drained using a coagulation bath rather than evaporating [41].

Effect of needle-to-Collector distance on fiber diameter

The tip-to-Collector distance can impact the fiber quality; beads may be seen if the tip-to-collector distance needs to be longer or longer. For this investigation were measured the TIP-to-collector distances between the range of 4 and 18 cm. Since the solution needed more time to transform into the fiber at the spread between 0-4 cm, producing fiber with the specified concentration was not realizable. On the other hand, a high distance (over 18 cm) from the collector has the same result due to the insufficient power to retire the fibers; the jets were sprayed where the tip-to-collector distance was greater than 18 cm.

The general trend reveals an increase in fiber diameter with increasing the tip-to-collector distance up to 13 cm, at this point, it achieves a plateau, as shown in *Figure 5-18* for the concentration of 12,5 w/v % CA. When the tip-to-collector distance was increased from 9 to 18 cm, the average fiber diameter for the 14 w/v % CA concentration went from 3,46 mm to 3,85 mm. The fiber diameter increased from 2,05 mm to 3,64 mm with an increase of 4 to 13 cm in the tip-to-collector distance. The extensive range of diameter uncertainty points to a weak relationship between average fiber diameter and tip-to-collector distance [61]. The expansion of the fiber diameter range may also be linked to the rise in bending instability. The whipping continuously changes the fibers' travel path, directly affecting the final fiber size. A similar study, however, came to the opposite conclusion, finding that the deposition range between 5 and 15 cm had no appreciable impact on the fibers' diameter, size, and shape [61].

Effect of voltage on Fiber diameter

A high voltage could lead to a lower fiber diameter when the tip-collector distance is sufficient to allow for more excellent jet extension. On the other hand, a high voltage can cause an increase in fiber diameter if a high polymer concentration or a short spinning distance prevents the jet from extending significantly. The circumstances to reduce fiber diameter should be found outside the experimented ranges, where it is unknown whether they are feasible or electro-spinnable. Smaller fiber diameters could have resulted from a decreased CA concentration [41].

Effect of Electrical Polarity on fiber diameter

Electrical polarity impacts the morphology and diameter of electrospun polymer fibers, relative humidity, solvent choice, and polymer concentration adjustments. The most used technique for evaluating the morphology of polymer fibers is scanning electron microscopy (SEM). According to a study [2], compressive electrospinning was performed on Type B gelatin dissolved in water and ethanol, chitosan dissolved in trifluoroacetic acid (TFA) and dichloromethane (DCM), PLGA dissolved in acetone, and PBT dissolved in 1-Hexafluoro-2-propanol (HF2P). Apart from chitosan (CHT), all polymer solutions formed fibers when negative voltage polarity was supplied. SEM analysis of the fiber quality revealed smooth and beaded morphologies. The average fiber diameter measurement for all polymer solutions shows thinner fibers produced with positive voltage. Interestingly, despite increased applied voltage increases, the fiber diameter remained constant for negative polarities [42].

In contrast, studies on PHBV dissolved in chloroform [2] revealed thicker PHBV fibers, measuring 2.9 μm for positive voltage and 1.5 μm for negative voltage of 15 kV. This effect was observed as the voltage was raised from 15 to 25 kV, increasing fiber diameters to 3.9 μm for negative voltage and 1.7 μm for positive voltage. In contrast, in a different study, [66] the morphology of PHBV fibers (dissolved in chloroform and N, N-dimethylformamide (DMF)) was similar regardless of the applied voltage polarity, producing smooth fibers with an equal fiber diameter of 2.840.22 μm for PHBV+ and 2.840.13 μm for PHBV-.

8.2 Effect of CA-microfiber composite on the properties of the paste

8.2.1 Compressive strength

Table 8-1 and *Figure 8-1* display the compressive strength of the cement pastes after 7d and 28d of curing. The 7d compressive strength of the reference sample was about 46.0 MPa. A higher compressive strength was observed when CA-microfibers were used. The 7d Compressive strengths for the cement pastes containing 0.1%, 0.5%, and 1% CA-microfibers were 50.8 MPa, 48.9 MPa, and 53.4 MPa, respectively. It is clear that the highest compressive strength was achieved by adding 1% CA microfiber *Table 8-1* compared to the reference; the compressive strength has increased by 13.9%. The 28d compressive strength of cement paste containing CA nanofibers at various concentrations (0%, 0.1%, 0.5%, and 1.0%) is presented in *Table 8-1*. In contrast to the 7d strength results, CA resulted in a decrease in compressive strength compared to the reference paste. For instance, the compressive strength of the sample with 0%, 0.1%, 0.5%, and 1.0%CA was about 72.4 MPa, 60.6 MPa, 52.9 MPa, and 67.1 MPa, respectively.

Table 8-1 Compressive strength test results at 7d and 28d.

Samples	No.	Fiber content	water ratio	Curing condition	7d-Compressive strength		28-Compressive strength	
					[MPa]	Average [MPa]	[MPa]	Average [MPa]
Reference	1.1	0.00%	0.4	20°C in water	53.7	46.0	72.0	72.4
	1.2				42.1		72.2	
	1.3				42.1		72.9	
0.1% CA	2.1	0.10%			54.8	50.8	59.5	60.6
	2.2				58.8		60.0	
	2.3				38.9		62.4	
0.5% CA	3.1	0.50%			35.1	48.9	48.4	52.9
	3.2				56.9		60.6	
	3.3				54.6		49.7	
1% CA	4.1	1.00%			54.2	53.4	64.3	67.1
	4.2				59.3		70.2	
	4.3				46.8		66.8	

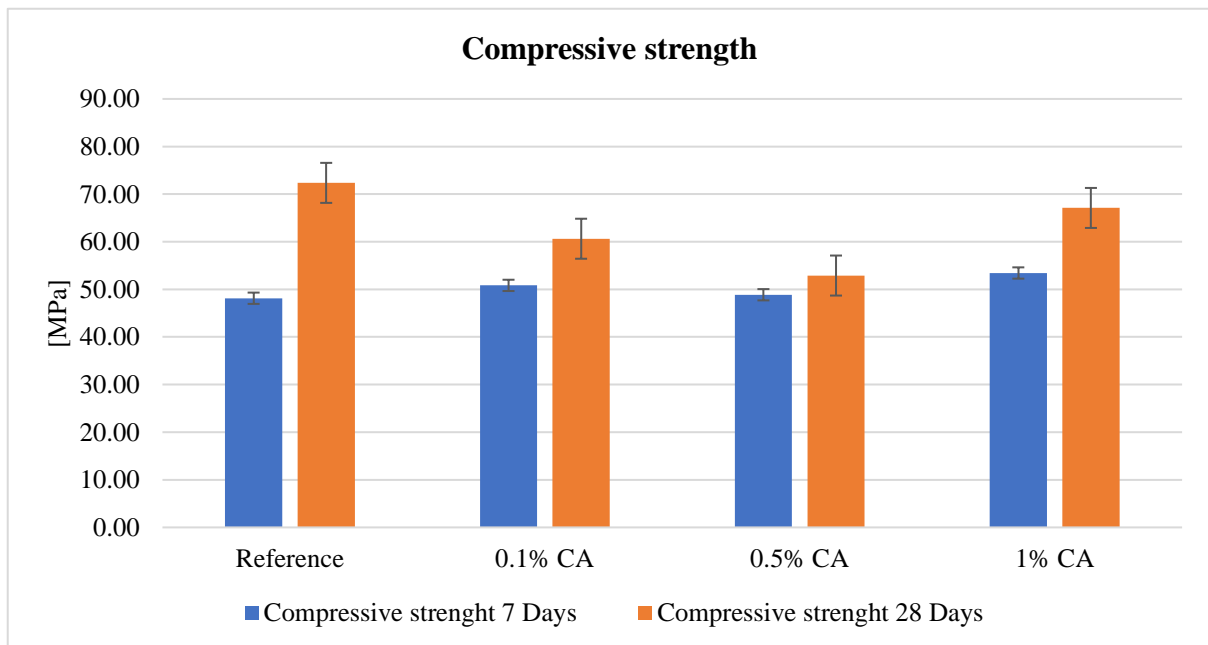


Figure 8-1 Compressive strength result for 7d and 28d.

To the best of our knowledge, we have not found any articles that specifically present 7-day results for comparison with the current study. The available paper [29] related to this study only provides

findings after 28 days. Nevertheless, it is noteworthy that the higher compressive strength after 7d could be attributed to the increased interfacial interaction between CA fibers with the cement paste matrix. These results from this thesis align with similar research on the mechanical properties of cement paste composites reinforced with nanofibers. Several studies have examined nanofiber reinforcements' impact on cement paste composites' mechanical characteristics. For instance, according to Liu et al. [69], carboxymethyl cellulose increased the compressive strength of specimens made of cement mortar by up to 331%. Similar findings were made by Dianah et al.[68], who discovered that cellulose nanocrystals enhanced the compressive strength of cement-based composites after 7d. Additionally, recent work by [70] examined the impact of carbon nanofibers on the mechanical properties of cement paste. They reported that adding carbon nanofibers increased the composite's compressive strength. Overall, the findings of this experiment show that CA microfibers could improve the compressive strength at the early age of cement paste. The higher compressive strength after 7d could be attributed to the increased interfacial interaction between CA fibers with the cement paste matrix.

The 28d compressive strength findings are inconsistent with other research on using CA microfibers in cement composites. Previous studies [29] have found that adding nanofibers to cement increased the 28d compressive strength. They have attributed this mainly due to the mechanical properties of electrospun CA fibers, a high surface-to-volume ratio, and exhibit good dispersion in water. Furthermore, other contributing factors may include their moderate hydrophilicity, which is induced using a surfactant. However, it is important to note that the influence of surfactant was not considered in our study.

The reduction in 28-day compressive strength observed in this study can be attributed to another factor, namely the water/cement ratio. This study employed the same water/cement ratio for all four fiber concentrations. Although there was room for improvement in the water/cement ratio, it was not possible to address this issue in this thesis due to constraints in fiber production. In order to reduce the risk of running out of fiber, the students decided to maintain a consistent water/cement ratio. This choice was influenced by the limited time available for fiber production, which posed a potential challenge in improving the water/cement ratio.

8.2.2 Flexural strength

Table 8-2 and *Figure 8-2* provide an overview of the flexural strength of the cement pastes after 7 days and 28 days of curing. The reference sample exhibited a 7-day flexural strength of approximately 6.8 MPa. However, when CA-microfibers were incorporated, a lower flexural strength was observed.

Specifically, the 7-day flexural strengths for cement pastes containing 0.1%, 0.5%, and 1% CA-microfibers were 5.0 MPa, 5.7 MPa, and 4.7 MPa, respectively. The addition of CA microfibers did not lead to an increase in flexural strength compared to the reference. The 28-day compressive strength of cement paste containing various concentrations (0%, 0.1%, 0.5%, and 1.0%) of CA nanofibers is presented. Similar to the 7-day results, the inclusion of CA nanofibers did not enhance the flexural strength when compared to the reference paste. For example, the flexural strength values for samples with 0%, 0.1%, 0.5%, and 1.0% CA were approximately 6.8 MPa, 4.9 MPa, 5.8 MPa, and 4.1 MPa, respectively.

Table 8-2 Flexural strength test results at the age of 7d and 28d

Samples	No.	Fiber content	water ratio	Curing condition	7d-Flexural strength		28d-Flexural strength	
					[MPa]	Average [MPa]	[MPa]	Average [MPa]
Reference	1.1	0.00%	0.4	20°C in water	6.9	6.7	6.6	6.8
	1.2				6.6		7.0	
	1.3				6.8		6.8	
0.1% CA	2.1	0.10%			4.7	5.0	5.2	4.9
	2.2				5.1		4.7	
	2.3				5.2		4.9	
0.5% CA	3.1	0.50%			5.0	5.7	5.5	5.8
	3.2				5.4		6.2	
	3.3				6.7		5.8	
1% CA	4.1	1.00%			4.9	4.7	3.9	4.1
	4.2				3.4		4.3	
	4.3				5.9		4.2	

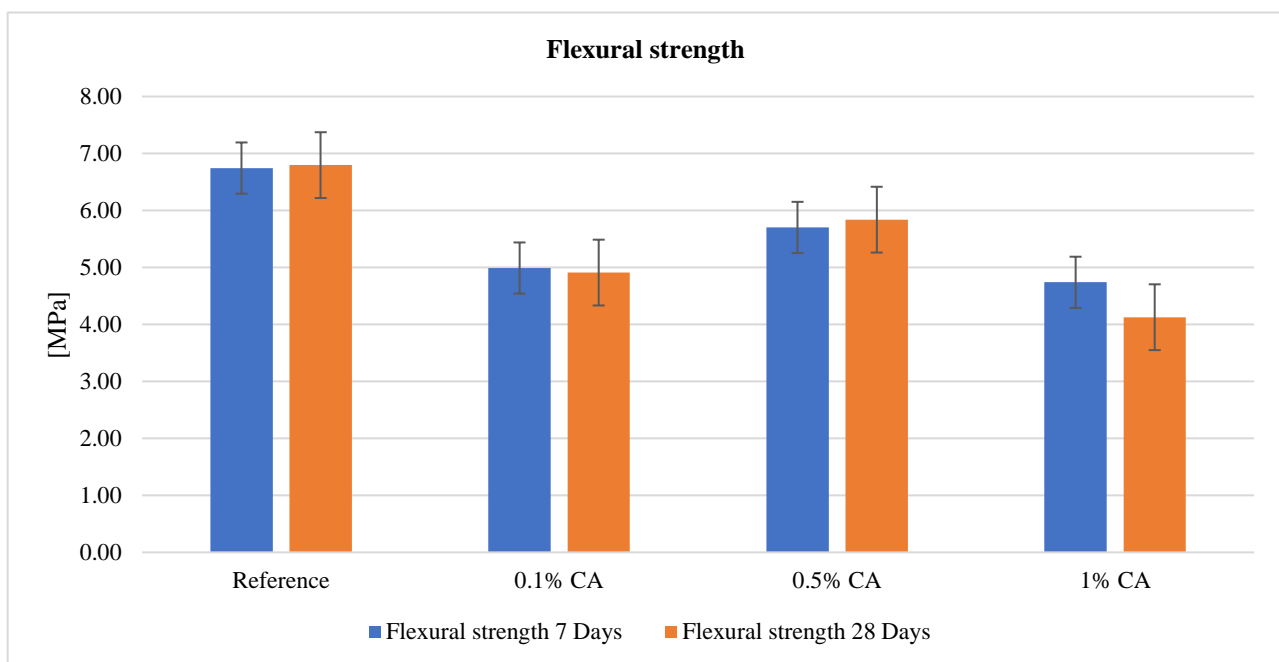


Figure 8-2 Result for the flexural strength result for 7d and 28d.

The agglomeration of cellulose microfibers, leading to an uneven dispersion of fibers within the cement matrix, could contribute to the observed loss in strength. This agglomeration of fibers phenomenon occurs due to the localization of a substantial amount of fibers and the subsequent formation of interconnected networks. These agglomerated CA fibers give rise to regions of weak spots in the form of pores [78]. During the curing process, these agglomerated fibers act as stress concentrators within the cementitious matrix *Figure 8-3*, thereby promoting the occurrence of premature cracking [79].

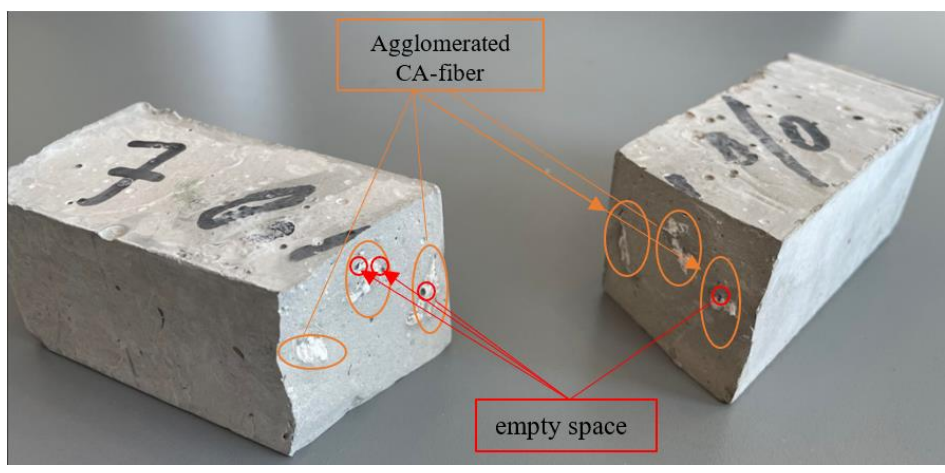


Figure 8-3 Observed agglomerated CA-fiber and weak spots in the cement samples after being tested.

Agglomeration of the fibers can also be supported with SEM (Scanning Electron Microscope) images *Figure 8-4*. The images were captured from samples with different concentrations of CA (0.5% and 1%). Specifically, images (a) and (b) were taken from the same sample with a 1% CA concentration. In the image (a), the agglomeration of fibers is clearly visible, indicating clumps of fibers within the model. However, image (b) has no visible fibers despite being taken from the same sample. This disparity in fiber visibility suggests that agglomeration of the fibers is present in the image (a). In contrast, in the image (b), the fibers appear uniformly dispersed without any noticeable agglomeration. These SEM images visually confirm the varying degree of fiber agglomeration in the samples with different CA concentrations, highlighting the potential presence of agglomerated regions or weak spots within the cement matrix.

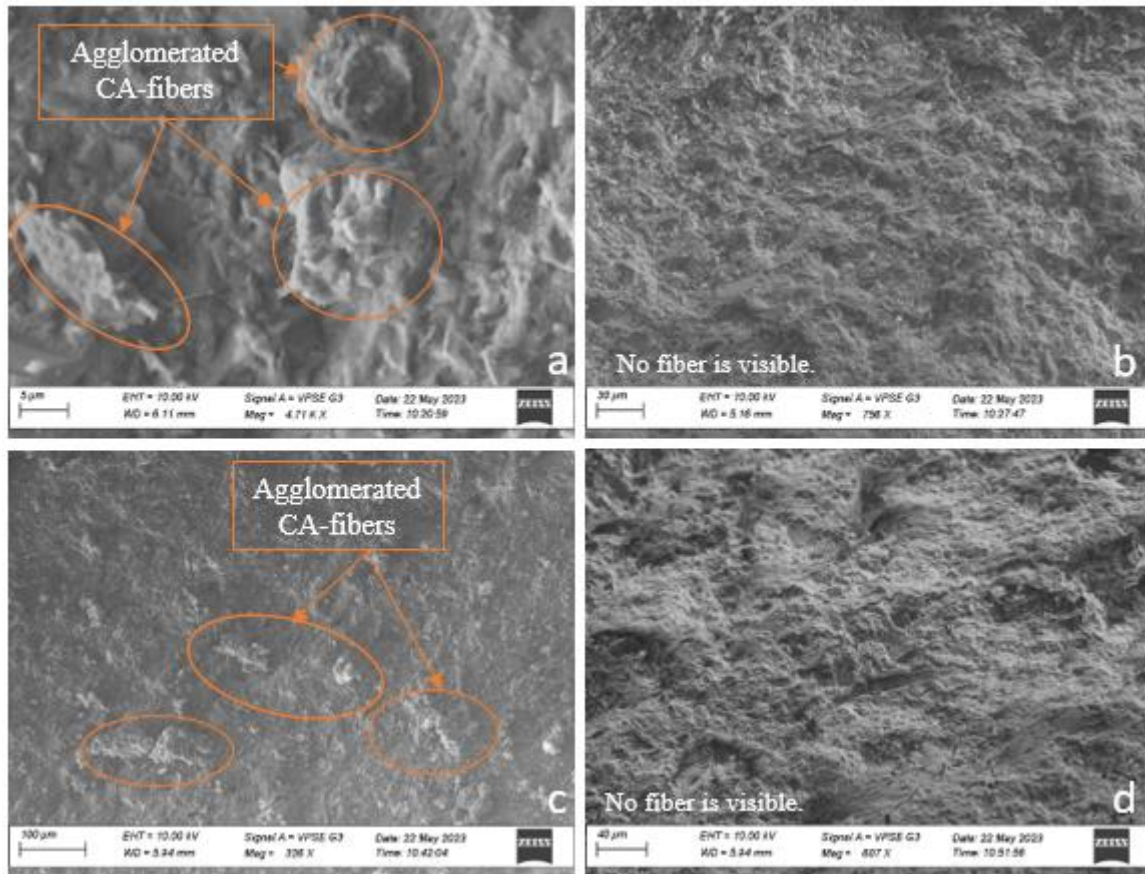


Figure 8-4 SEM images of the samples containing 0.5% CA (c & d) and 1% CA (a & b). Images (a) & (c) visible agglomeration of fibers. Images (b) & (d) show no observable fibers.

The observed drop in flexural strength can be explained by excessive microfiber content, which can affect the mechanical properties. *Figure 8-5* presents the average peak load for three tests, accompanied by standard deviation error bars, to illustrate the evolution of peak load over time.

Across all sample ages, a consistent decrease in peak load is observed in samples containing 0.1%, 0.5%, and 1% CA microfibers. In a study conducted by Onuaguluchi et al. [78], it was noted that beyond an addition level of 0.1% cellulose microfibers, the agglomeration of fibers hurt strength enhancement, particularly at the 0.4% content level. At this specific addition level, the strength fell below the control samples. Furthermore, Cao et al. [80] demonstrated that the material's strength peaks at approximately 0.2% of cellulose nanocrystals (CNC) and subsequently declines.

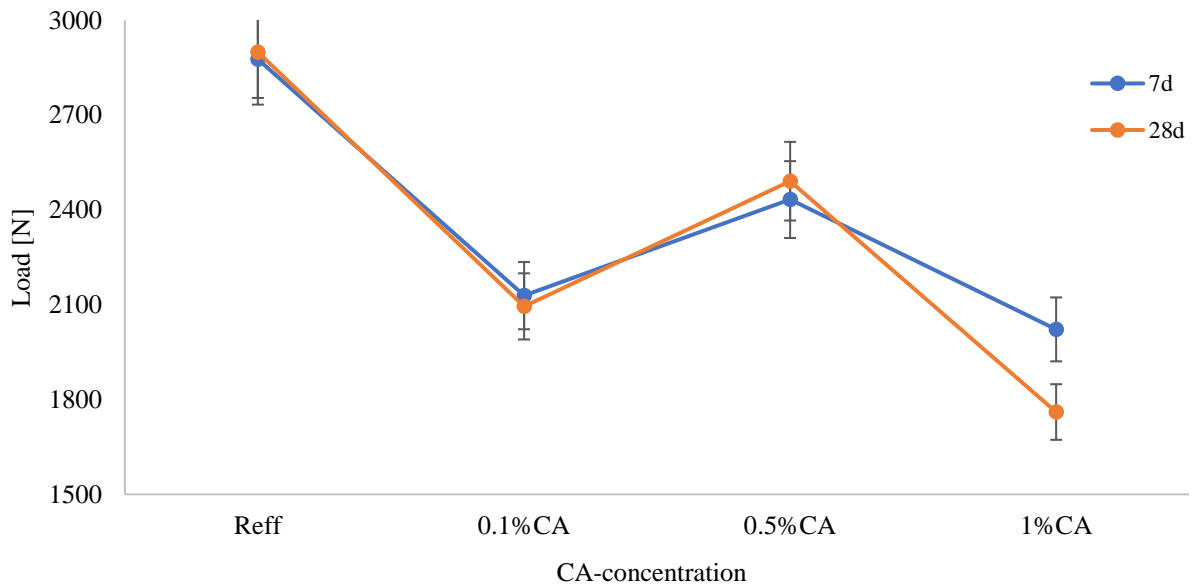


Figure 8-5 Average Peak load at 7d and 28d

Figure 8-6 shows the Load versus Deformation test outcomes for the 28-day samples. With the addition of 0.5% CA, it exhibits an initial peak load approximately higher than the reference mixtures. However, it decreases at the next peak load. On the other hand, the addition of 0.1% and 1% CA shows a noticeable reduction in the peak load. This peak load reduction could be attributed to the agglomeration of CA microfibers within the mixture, which hinders their effective reinforcement.

Moreover, in the CA samples, the rate of load increase is comparatively lower than that observed in the reference samples. This discrepancy in load rate could be due to the inconsistency in crack size. It has been observed that, for all CA samples, the width of the cracks is more comprehensive than 0.3 mm. This widening of cracks may be influenced by factors such as shrinkage, particularly in regions with the highest concentration of CA microfibers. Higher concentrations of CA microfibers may contribute to increased shrinkage, leading to wider cracks and potentially compromising the overall sample integrity [81].

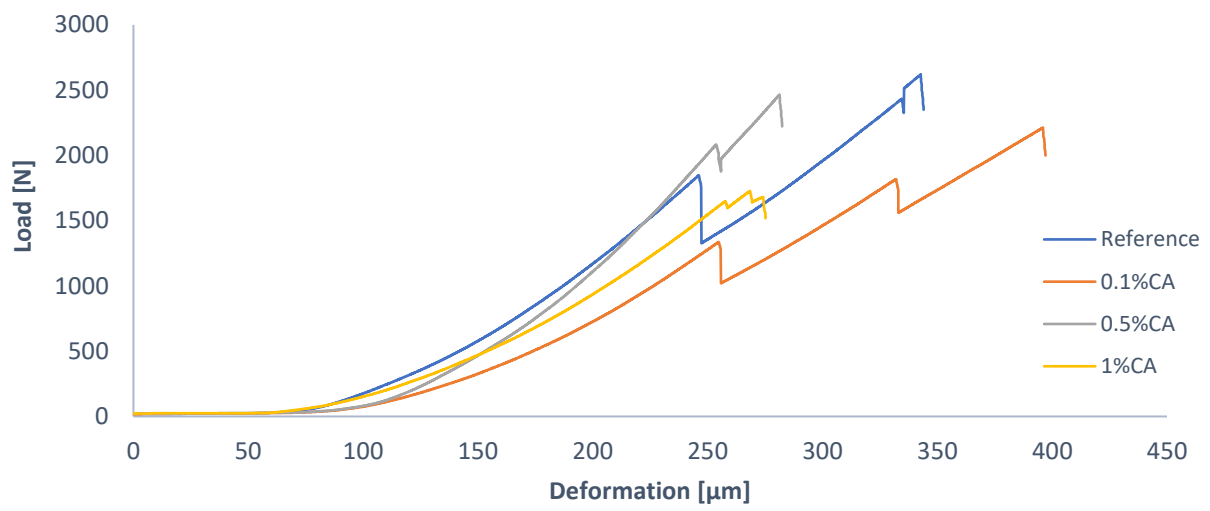


Figure 8-6 Load versus Deformation at 28d

9 Conclusion

The experimental portion of the electrospinning procedure in this thesis looked at how the various parameters mentioned in section (3.5) affected the diameter size of the microfiber, which was the research objective. A rigorous series of experiments were run using a quantitative approach, and the results led to the production of microscale fibers.

The experimental data analysis indicated numerous significant correlations and patterns between the distance and diameter. The results for the CA microfibers, particularly in the CA/Aceton combination of 12.5g and 100 ml, were entirely at odds with those of Zheng-Ming, H. et al. [1]. Wich discovered that increasing the jetes' traveling distance in electrospinning increases the fiber's diameter while allowing the solvent more time to evaporate. While the voltage versus diameter experimental splits to result where the outcome for the positive high voltage charge supports the discovery of Wu et al. (2012) [64], increasing voltage reduced fiber diameters to a minimum before the trend reversed with further voltage increase. On the other side, the negative high voltage charge Mazoochi et al. 2012 [64] claim initially increases fiber diameter, but the fiber diameter begins to decrease after a specific voltage. Lastly, the flow rate effect shows almost the same trend and correlation in both negative and positive high voltage charges, where the diameter of the fibers remains minor until a specific flow range, and the diameter of the fiber begins to increase.

Lastly, regardless of the high voltage charge's polarity, the flow rate's effect on the electrospinning process exhibits consistent trends and correlations. In particular, it was shown that the fibers' diameter stays constant mainly within a range of flow rates but starts to rise outside of this range. In order to obtain the appropriate fiber morphology and prevent the creation of beads or inconsistent fibers, it is imperative to choose an ideal flow rate range. It is crucial to remember that our research cannot definitively state what flow rate range is best.

Our results also show that the material's qualities impact the flow rate effect. While more viscous solutions like Polyvinylpyrrolidone/Tetraethyl Orthosilicate (PVP/TEOS) require a lower flow rate range, low-viscosity solutions like Cellulose Acetate-Acetone (CA) demand a more extensive flow rate range. For instance, the CA solution needed a flow rate between 1.6 ml/hr and 5 ml/hr to start producing fiber, but the PVP/TEOS solution produced a minor fiber diameter at a flow rate of 0.8 ml/hr. However, it is essential to note that the diameter for CA began to increase at 1.6 ml/hr, and at 5 ml/hr, it rose quickly.

Our investigation into the interactions between flow rate and fiber diameter during electrospinning has revealed important new information. Even though we have seen material-dependent

characteristics and patterns, more analysis is required to establish clear criteria for choosing flow rates. Understanding the unique characteristics of the flow rate impact can help in electrospinning parameter optimization, enabling the creation of consistent and desired fiber morphologies for a variety of applications.

In summary, this thesis developed Cellulose Acetate CA microfibers through an electrospinning technique using the most promising parameter to produce the minor diameter. The novel product utilized for the further experiment has an average diameter of 2,27 μm received by the flow rate of 1.6 ml/hr, voltage +15 kV, and distance of 10cm.

The compressive strength results indicate that adding CA microfibers to the cement paste can enhance the early-age compressive strength. Specifically, at 7 days of curing, the samples containing 0.1%, 0.5%, and 1% CA microfibers exhibited higher compressive strength than the reference sample. The highest compressive strength was achieved with 1% CA microfiber, resulting in a 13.9% increase compared to the reference.

However, the 28-day compressive strength results showed a decrease in strength for the CA samples compared to the reference. This contrast in findings may be attributed to factors such as the agglomeration of fibers and the water/cement ratio. The agglomeration of cellulose microfibers within the cement matrix leads to uneven dispersion and the formation of weak spots in the form of pores, which can adversely affect the strength. SEM images supported this observation, showing varying degrees of fiber agglomeration in samples with different CA concentrations.

The flexural strength results revealed a consistent reduction in peak load for all CA samples, indicating a negative impact of excessive microfiber content on the mechanical properties. The rate of load increase in the CA samples was lower, possibly due to inconsistent crack sizes, with wider cracks observed in regions with higher CA microfiber concentrations. Factors like shrinkage may influence this widening of cracks.

These findings suggest that while CA microfibers can enhance early-age compressive strength, they may have limitations in improving long-term flexural strength due to agglomeration and other factors. Further investigation is needed to optimize the fiber dispersion and water/cement ratio to mitigate these challenges and maximize the potential benefits of CA microfibers in cement composites.

10 Recommendations for future work

Several improvements could be considered in future works in order to achieve better results. In the following, some of the open issues that deserve further research will be presented:

1. The solutions adopted in this research are based on CA and PVP/TEOS, chosen based on earlier studies (see Chapter 4). The PVP/TEOS electrospun showed weak water resistance. In other words, the electrospun manufactured during the experiment dissolved afterward when immersed in water. The authors try to improve the quality of the solution (see section (4.2)) but fail to succeed. The authors highly recommend a deeper study of the chemical state to ensure a sustainable solution.
2. Investigating alternative strategies for introducing microfiber mats into cement paste to enhance the distribution of the microfiber and create a uniformly distributed cement matrix. For instance, pre-treatment of the electrospun to separate the fiber mesh might increase the opportunity to develop a better matrix.
3. More research is needed to enhance the mixing process and the dispersion of microfibers within the cement. With a deeper understanding of the underlying mechanics and more experimentation, it may overcome the challenges of microfiber dispersion and produce more potent and resilient building materials.
4. The workability of the electrospun fiber-reinforced cementitious materials can be an issue in the future. Since the construction industry
5. The specimen preparation was performed according to the standard (see Chapter (7)), and the author's speculation also goes to the curing strategy adopted. Since the samples were cured in water and no research was done in this area. Further study on the polymer reaction to the cement hydration process and adherence level, whether it could be satisfactory, curing outside water in contrast to the curing in the water.

11 Reference

1. Zheng-Ming, H., et al., *A review on polymer nanofibers by electrospinning and their applications in nanocomposites*. Composites Science and Technology, 2003. **63**(15): p. 2223-2253.
2. Xue, J., et al., *Electrospinning and electrospun nanofibers: Methods, materials, and applications*. Chemical Reviews, 2019. **119**(8): p. 5298-5415.
3. Yarin, A.L., S. Koombhongse, and D.H. Reneker, *Taylor cone and jetting from liquid droplets in electrospinning of nanofibers*. Journal of applied physics, 2001. **90**(9): p. 4836-4846.
4. Taylor, G.I., *Disintegration of water drops in an electric field*. Proceedings of the Royal Society of London. Series A. Mathematical and Physical Sciences, 1964. **280**(1382): p. 383-397.
5. Mortimer, C.J. and C.J. Wright, *The fabrication of iron oxide nanoparticle-nanofiber composites by electrospinning and their applications in tissue engineering*. Biotechnology journal, 2017. **12**(7): p. 1600693.
6. Khalf, A. and S.V. Madihally, *Recent advances in multiaxial electrospinning for drug delivery*. European Journal of Pharmaceutics and Biopharmaceutics, 2017. **112**: p. 1-17.
7. Islam, M.S., et al., *A review on fabrication of nanofibers via electrospinning and their applications*. SN Applied Sciences, 2019. **1**(10): p. 1248.
8. Xu, H., *Formation and characterization of polymer jets in electrospinning*. 2003.
9. Williams, G.R., B.T. Raimi-Abraham, and C.J. Luo, *Electrospinning fundamentals*, in *Nanofibres in Drug Delivery*. 2018, UCL Press. p. 24-59.
10. Sun, Z., et al., *The effect of solvent dielectric properties on the collection of oriented electrospun fibers*. Journal of Applied Polymer Science, 2012. **125**(4): p. 2585-2594.
11. Collins, R.T., et al., *Electrohydrodynamic tip streaming and emission of charged drops from liquid cones*. 2008. **4**(2): p. 149-154.
12. Begum, H.A. and K. Khan, *Study on the various types of needle based and needleless electrospinning system for nanofiber production*. Int. J. Text. Sci, 2017. **6**(8).
13. Jaworek, A., et al., *Electrostatic interaction of free EHD jets*. 2006. **40**(4): p. 568-576.
14. Jasikova, D., M. Kotek, and V. Kopecky, *The Investigation of the Industrial Spray Systems Using Interferometry Particle Imaging Method*. American Journal of Mechanical Engineering, 2013. **1**(7): p. 384-389.
15. Reneker, D.H., et al., *Advances in applied mechanics*. 2007. **41**: p. 43-195.
16. Reneker, D.H. and A.L. Yarin, *Electrospinning jets and polymer nanofibers*. 2008. **49**(10): p. 2387-2425.
17. Tech, E. *Centrifugal Electrospinning*. [cited 2022 15. Nov]; Available from: http://electrospintech.com/electroblowing.html#.WcJ3_DVx.
18. Bakar, S.S.S., et al., *Effect of Voltage and Flow Rate Electrospinning Parameters on Polyacrylonitrile Electrospun Fibers*. IOP Conference Series: Materials Science and Engineering, 2018. **318**(1): p. 012076.
19. Ding, W., et al., *Manipulated electrospun PVA nanofibers with inexpensive salts*. Macromolecular Materials and Engineering, 2010. **295**(10): p. 958-965.
20. Helgeson, M.E., et al., *Theory and kinematic measurements of the mechanics of stable electrospun polymer jets*. Polymer, 2008. **49**: p. 2924-2936.
21. Reneker DH, F.H., Eds, *Polymeric Nanofibers*, ed. A. Symposium. Vol. 918. 2006, Washington, DC, USA,: American Chemical Society.
22. Ramakrishna, S., et al., *Introduction To Electrospinning And Nanofibers*, An. 2005, Singapore, SINGAPORE: World Scientific Publishing Company.
23. Gea, S., et al., *Carbon-Nano Fibers Yield Improvement with Iodinated Electrospun PVA/Silver Nanoparticle as Precursor via One-Step Synthesis at Low Temperature*. Polymers, 2022. **14**(3): p. 446.
24. Korotcenkov, G., *Electrospun Metal Oxide Nanofibers and Their Conductometric Gas Sensor Application. Part 1: Nanofibers and Features of Their Forming*. Nanomaterials, 2021. **11**(6): p. 1544.
25. Pantojas, V., et al., *Synthesis of Palladium with Different Nanoscale Structures by Sputtering Deposition onto Fiber Templates*. Departmental Papers (ESE), 2008. **2**.

26. Wang, G., et al., *Electrospun nanofiber: Emerging reinforcing filler in polymer matrix composite materials*. Progress in Polymer Science, 2017. **75**: p. 73-107.
27. Nguyen, T.N.M., D.-Y. Yoo, and J.J. Kim, *Cementitious material reinforced by carbon nanotube-Nylon 66 hybrid nanofibers: Mechanical strength and microstructure analysis*. Materials Today Communications, 2020. **23**: p. 100845.
28. Izaguirre, A., J. Lanás, and J.I. Alvarez, *Effect of a polypropylene fibre on the behaviour of aerial lime-based mortars*. Construction and Building Materials, 2011. **25**(2): p. 992-1000.
29. Chousidis, N., et al., *Mechanical Reinforcement of Lime Pastes by Electrospun Cellulose Acetate Polymer Fibers*. Fibers and Polymers, 2021. **22**: p. 1-9.
30. Nguyen, T., D. Lee, and J. Kim, *Effect of Electrospun Nanofiber Additive on Selected Mechanical Properties of Hardened Cement Paste*. Applied Sciences, 2020. **10**: p. 7504.
31. Reneker, D.H., et al., *Nanofiber garlands of polycaprolactone by electrospinning*. Polymer, 2002. **43**: p. 6785-6794.
32. Ngiam, M., et al., *The fabrication of nano-hydroxyapatite on PLGA and PLGA/collagen nanofibrous composite scaffolds and their effects in osteoblastic behavior for bone tissue engineering*. Bone, 2009. **45**(1): p. 4-16.
33. Kramar, A. and F.J. González-Benito, *Cellulose-Based Nanofibers Processing Techniques and Methods Based on Bottom-Up Approach-A Review*. Polymers (Basel), 2022. **14**(2).
34. Villiger-Oberbek, A., et al., *Development and application of a high-throughput platform for perfusion-based cell culture processes*. Journal of Biotechnology, 2015. **212**: p. 21-29.
35. Tijing, L.D., et al., *1.16 Electrospinning for Membrane Fabrication: Strategies and Applications, in Comprehensive Membrane Science and Engineering (Second Edition)*, E. Drioli, L. Giorno, and E. Fontananova, Editors. 2017, Elsevier: Oxford. p. 418-444.
36. Huang, Y., et al., *Scalable manufacturing and applications of nanofibers*. Materials Today, 2019. **28**: p. 98-113.
37. Long, Y.-Z., et al., *Chapter 2 - Electrospinning: The Setup and Procedure, in Electrospinning: Nanofabrication and Applications*, B. Ding, X. Wang, and J. Yu, Editors. 2019, William Andrew Publishing. p. 21-52.
38. He, J.-H., Y. Wu, and W.-W. Zuo, *Critical length of straight jet in electrospinning*. Polymer, 2005. **46**(26): p. 12637-12640.
39. Prabu, G.T.V., et al., *Process optimization and modelling the BET surface area of electrospun cellulose acetate nanofibres using response surface methodology*. Bulletin of Materials Science, 2022. **45**(3): p. 133.
40. Hekmati, A.H., et al., *Effect of needle length, electrospinning distance, and solution concentration on morphological properties of polyamide-6 electrospun nanowebs*. Textile Research Journal, 2013. **83**(14): p. 1452-1466.
41. Angel, N., et al., *Effect of processing parameters on the electrospinning of cellulose acetate studied by response surface methodology*. Journal of Agriculture and Food Research, 2020. **2**: p. 100015.
42. Ura, D. and U. Stachewicz, *The Significance of Electrical Polarity in Electrospinning: A Nanoscale Approach for the Enhancement of the Polymer Fibers Properties*. Macromolecular Materials and Engineering, 2022. **307**.
43. Ying Yang, et al., *THE EFFECTS OF FLOW RATE AND THE DISTANCE BETWEEN THE NOZZLE AND THE TARGET ON THE OPERATING CONDITIONS OF ELECTROSPINNING*. Journal of Polymer Engineering, 2008. **28**(1-2): p. 67-86.
44. Zargham, S., et al., *The Effect of Flow Rate on Morphology and Deposition Area of Electrospun Nylon 6 Nanofiber*. Journal of Engineered Fibers and Fabrics, 2012. **7**: p. 42-49.
45. Syed Bakar, S., et al., *Effect of Voltage and Flow Rate Electrospinning Parameters on Polyacrylonitrile Electrospun Fibers*. IOP Conference Series: Materials Science and Engineering, 2018. **318**: p. 012076.
46. Frontera, P., et al., *Manufacturing and Assessment of Electrospun PVP/TEOS Microfibres for Adsorptive Heat Transformers*. Coatings, 2019. **9**(7): p. 443.
47. Liu, H. and Y.-L. Hsieh, *Ultrafine fibrous cellulose membranes from electrospinning of cellulose acetate*. Journal of Polymer Science Part B: Polymer Physics, 2002. **40**(18): p. 2119-2129.
48. Tungprapa, S., et al., *Electrospun cellulose acetate fibers: effect of solvent system on morphology and fiber diameter*. Cellulose, 2007. **14**(6): p. 563-575.

49. Celebioglu, A. and T. Uyar, *Electrospun porous cellulose acetate fibers from volatile solvent mixture*. Materials Letters, 2011. **65**(14): p. 2291-2294.
50. Srinivasan, G.K. and D.H. Reneker, *Structure and morphology of small diameter electrospun aramid fibers*. Polymer International, 1995. **36**: p. 195-201.
51. Shin, Y.M., et al., *Experimental characterization of electrospinning: the electrically forced jet and instabilities*. Polymer, 2001. **42**: p. 09955-09967.
52. Shenoy, S.L., et al., *Role of chain entanglements on fiber formation during electrospinning of polymer solutions: Good solvent, non-specific polymer-polymer interaction limit*. Polymer, 2005. **46**: p. 3372-3384.
53. Fong, H., I. Chun, and D.H. Reneker, *Beaded nanofibers formed during electrospinning*. Polymer, 1999. **40**(16): p. 4585-4592.
54. Buchko, C.J., K.M. Kozloff, and D.C. Martin, *Surface characterization of porous, biocompatible protein polymer thin films*. Biomaterials, 2001. **22**(11): p. 1289-300.
55. Chen, P., et al., *Biomimetic composite scaffold of hydroxyapatite/gelatin-chitosan core-shell nanofibers for bone tissue engineering*. Mater Sci Eng C Mater Biol Appl, 2019. **97**: p. 325-335.
56. Ou, Q., et al., *Zein/gelatin/nanohydroxyapatite nanofibrous scaffolds are biocompatible and promote osteogenic differentiation of human periodontal ligament stem cells*. Biomaterials Science, 2019. **7**(5): p. 1973-1983.
57. Llorens, A., et al., *Metallic-based micro and nanocomposites in food contact materials and active food packaging*. Trends in Food Science & Technology, 2012. **24**(1): p. 19-29.
58. Nayab-Ul-Hossain, A.K.M., et al., *Preparation of graphene based natural fiber (Jute)-synthetic fiber (Glass) composite and evaluation of its multifunctional properties*. Composites Part C: Open Access, 2022. **9**: p. 100308.
59. Mikaeili, F. and P.I. Gouma, *Super water-repellent cellulose acetate mats*. Scientific reports, 2018. **8**(1): p. 12472.
60. Matos, R.J., et al., *Electrospun composite cellulose acetate/iron oxide nanoparticles non-woven membranes for magnetic hyperthermia applications*. Carbohydrate polymers, 2018. **198**: p. 9-16.
61. Ahne, J., et al., *Electrospun cellulose acetate nanofibers for airborne nanoparticle filtration*. Textile Research Journal, 2018. **89**(15): p. 3137-3149.
62. Shafieifar, M., M. Farzad, and A. Azizinamini, *Experimental and numerical study on mechanical properties of Ultra High Performance Concrete (UHPC)*. Construction and Building Materials, 2017. **156**: p. 402-411.
63. AlMaadeed, M.A.A., D. Ponnamma, and A.A. El-Samak, *Chapter 1 - Polymers to improve the world and lifestyle: physical, mechanical, and chemical needs*, in *Polymer Science and Innovative Applications*, M.A.A. AlMaadeed, D. Ponnamma, and M.A. Carignano, Editors. 2020, Elsevier. p. 1-19.
64. Yun-Ze, L., et al., *Chapter 2 - Electrospinning: The Setup and Procedure*. Micro and Nano Technologies, 2019: p. 21-52.
65. Son, W.K., et al., *Electrospinning of ultrafine cellulose acetate fibers: studies of a new solvent system and deacetylation of ultrafine cellulose acetate fibers*. Journal of Polymer Science Part B: Polymer Physics, 2004. **42**(1): p. 5-11.
66. Gherasim, O., et al., *Composite P(3HB-3HV)-CS Spheres for Enhanced Antibiotic Efficiency*. Polymers, 2021. **13**: p. 989.
67. Zunino, F., D.P. Bentz, and J. Castro, *Reducing setting time of blended cement paste containing high-SO₃ fly ash (HSFA) using chemical/physical accelerators and by fly ash pre-washing*. Cement and Concrete Composites, 2018. **90**: p. 14-26.
68. Dianah, M., et al., *Effect of Cellulose Nanocrystals Extracted from Oil Palm Empty Fruit Bunch as Green Admixture for Mortar*. Scientific Reports, 2020. **10**: p. 6412.
69. Liu, H., et al., *Improvement of compressive strength of lime mortar with carboxymethyl cellulose*. Journal of Materials Science, 2016. **51**.
70. Barbhuiya, S. and P. Chow, *Nanoscaled Mechanical Properties of Cement Composites Reinforced with Carbon Nanofibers*. Materials (Basel, Switzerland), 2017. **10**.
71. Sajedi, F. and H.A. Razak, *Effects of curing regimes and cement fineness on the compressive strength of ordinary Portland cement mortars*. Construction and Building Materials, 2011. **25**(4): p. 2036-2045.

72. Hamad, A.J., *Size and shape effect of specimen on the compressive strength of HPLWFC reinforced with glass fibres*. Journal of King Saud University - Engineering Sciences, 2017. **29**(4): p. 373-380.
73. Cramariuc, B., et al., *Fiber diameter in electrospinning process*. Journal of Electrostatics, 2013. **71**(3): p. 189-198.
74. NanoScience. *Electrospinning*. [cited 2022 12 november]; Available from: <https://www.nanoscience.com/>
75. Hasan, M., A.K.M.M. Alam, and K. Nayem, *Application of electrospinning techniques for the production of tissue engineering scaffolds: A Review*. European Scientific Journal, 2014. **10**.
76. Asmatulu, R., *Highly Hydrophilic Electrospun Polyacrylonitrile/ Polyvinylpyrrolidone Nanofibers Incorporated with Gentamicin as Filter Medium for Dam Water and Wastewater Treatment*. Journal of Membrane and Separation Technology, 2016. **5**: p. 38-56.
77. Singh, S. and A. Subramanian, *Phase-field simulations of electrohydrodynamic jetting for printing nano-to-microscopic constructs*. RSC Advances, 2020. **10**: p. 25022-25028.
78. Onuaguluchi, O., D.K. Panesar, and M. Sain, *Properties of nanofibre reinforced cement composites*. Construction and Building Materials, 2014. **63**: p. 119-124.
79. Mejdoub, R., et al., *Nanofibrillated cellulose as nanoreinforcement in Portland cement: Thermal, mechanical and microstructural properties*. Journal of Composite Materials, 2017. **51**(17): p. 2491-2503.
80. Cao, Y., et al., *The influence of cellulose nanocrystal additions on the performance of cement paste*. Cement and Concrete Composites, 2015. **56**: p. 73-83.
81. Ghahari, S., et al., *Fracture Properties Evaluation of Cellulose Nanocrystals Cement Paste*. Materials (Basel), 2020. **13**(11).

12 Appendix

1. **Appendix 1** Optical visualization of the electrospun examined in (Chapter 4)
2. **Appendix 2** CEM I declaration of performance
3. **Appendix 3** Laboratory result of compressive and flexural strength test